From Individuals to Continuum Mechanics

In the previous chapter, we discussed the conditions under the density $b_i(\mathbf{x}, t)$ of particular organisms/ species/ groups of species is an appropriate representation of the spatial distribution of individuals. But the same question arises in the dynamics: to what degree do we need to calculate where each individual is, what it is doing, what it may be eating, and what may be preying upon it? Or can we generate predictive equations for $\frac{\partial}{\partial t} b_i$, and when might such an approach fail? Our previous derivation of equations for the changes of the densities in time assumed that they were advected and diffused by the fluid flow in the same manner as inert tracers such as salinity. But an organism – even a "planktonic" organism – usually can move relative to the water, if only to sink or rise buoyantly. These behavioral motions may be quite large: some zooplankton can migrate up and down 1000 m vertically in a day, corresponding to a velocity several orders of magnitude higher than the vertical velocities in the fluid. In this chapter, we shall revisit the dynamics to see how the movements of organisms can result in aggregation, dispersal and/or translation of a group. We shall also see how the quantities characterizing the motion and spread (or convergence) of the density field are related to individual behavior.

The mathematics developed here apply to other problems where stochastic variability can be significant; in particular, we shall use the same ideas to study structured population models in Chapter xx.

2.1 — Importance of Movement

Currency-based reaction-advection-diffusion models in which motion and mixing are purely physical share one property: no matter how many compartments or how complex the interactions are, the total

$$b_T = \sum_i b_i$$

satisfies the same advection-diffusion equation as a passive tracer. By construction, we have accounted for all the exchanges of, say, nitrogen so that

$$\sum_i \mathcal{B}_i = 0 \quad ;$$

summing the individual biological equations gives

$$\frac{\partial}{\partial t} b_T + \mathbf{u} \cdot \nabla b_T = \nabla \cdot \kappa \nabla b_T \quad . \tag{2.1}$$

Equation 2.1 has important consequences:

- Local maxima or minima are smoothed out with time.
- If the values of b_T at the boundaries are held fixed, the maximum and minimum values will be found on the boundary.
- If there is no flux of material through the boundaries, b_T will become spatially and temporally uniform.

We can prove the first assertion by looking at the integral of b_T over a small area (volume) around a point $\mathbf{x}_0$

$$\frac{\partial}{\partial t}\int_A b_T = -\oint_{\partial A} \mathbf{u}\cdot\hat{\mathbf{n}}\, b_T + \oint_{\partial A} \kappa\hat{\mathbf{n}}\cdot\nabla b_T \quad .$$

If $\mathbf{x}_0$ is a local maximum, the last term will be negative definite, causing the peak value to decrease and, likewise, a minimum to be filled in. Defining the boundary of the area to be a contour of constant b_T allows us to show that the first term

$$-b_T|_{\partial A}\oint_{\partial A}\mathbf{u}\cdot\hat{\mathbf{n}} = -b_T|_{\partial A}\int_A \nabla\cdot\mathbf{u} = 0$$

vanishes for non-divergent flow. Since the advection does not contribute, the integrated value near a maximum will decrease with time.

The third assertion can be demonstrated by noting that the spatial average $\langle b_T\rangle$ is conserved

$$\begin{aligned}\frac{\partial}{\partial t}\langle b_T\rangle &= -\frac{1}{V}\int_A \nabla\cdot[\mathbf{u}b_T - \kappa\nabla b_T]\\ &= -\frac{1}{V}\oint_{\partial A}\hat{\mathbf{n}}\cdot[\mathbf{u}b_T - \kappa\nabla b_T]\\ &= 0 \quad .\end{aligned}$$

The deviation from the mean $b_T' = b_T - \langle b_T\rangle$ satisfies the same advection-diffusion equation. If we multiply said equation by b_T' and average, we find

$$\begin{aligned}\frac{\partial}{\partial t}\langle\frac{1}{2}b_T'^2\rangle &= -\frac{1}{V}\int_A \nabla\cdot[\mathbf{u}\frac{1}{2}b_T'^2] + \frac{1}{V}\int_A b_T'\nabla\kappa\nabla b_T'\\ &= -\frac{1}{V}\oint_{\partial A}\hat{\mathbf{n}}\cdot\mathbf{u}\frac{1}{2}b_T'^2 + \frac{1}{V}\oint_{\partial A} b_T'\kappa\hat{\mathbf{n}}\cdot\nabla b_T' - \frac{1}{V}\int_A \kappa|\nabla b_T'|^2\\ &= -\frac{1}{V}\int_A \kappa|\nabla b_T'|^2\end{aligned}$$

which shows that the variance around the spatial (and temporal) mean decreases steadily. Eventually, the total b_T will become uniform, invariant with respect to both $\mathbf{x}$ and t. The implications in the deep ocean are striking: almost all of b_T will be in the dissolved forms (e.g. nitrate plus nitrite) and the total of those would be uniform. Since observations indicate significant variability with large and systematic gradients, we cannot expect a closed model work well for an ocean basin.

Inhomogeneous sources or sinks for one or more constituents (e.g., riverine input of nutrients) can lead to inhomogeneous distributions for the same reasons that salinity is nonuniform – the variations on the top or sides will be advected into the interior and their amplitude will be attenuated, but not erased, by diffusion.

In addition, living creatures (or, for that matter, detrital material) move relative to the water; if we write a continuum equation for the i^{th} constituent

$$\frac{\partial}{\partial t}b_i + \nabla\cdot[(\mathbf{u}+\mathbf{u}_{bio,i})b_i - (\kappa+\kappa_{bio,i})\nabla b_i] = \mathcal{B}_i \quad ,$$

we find that the flux of b_T

$$\mathbf{u}b_T - \kappa\nabla b_T + \sum \mathbf{u}_{bio,i} b_i - \sum \kappa_{bio,i} \nabla b_i$$

depends on more than just b_T and its gradient. As we shall see, even relative simple types of motion can greatly alter the distribution of b_T. Movement can also produce aggregations or patches. For zooplankton (or fish, etc.), we can think of the reaction (birth, death, ...) terms in the density as being relatively small if we are considering times that are short compared to the life cycle. Localized, persistent, high density patches can arise when the biological component of the velocity $\mathbf{u}_{bio}$ is convergent.

With this background on the significance of motion relative to the water, we shall now examine models which help us understand the behavioral contribution to the velocity and to the diffusivity.

2.2 — Models of Stochastic Motion

To understand the effects of the behavior of organisms – their motion relative to the water – on their distribution, we start at the level of the individual and study its movements, both deterministic and stochastic. The common models for the position $\mathbf{X}$ of a single organism fall into two categories. In the simpler idealization, the animals make random hops (also called random walks)

$$\mathbf{X}(t+\delta t) = \mathbf{X}(t) + \mathbf{U}(t)\delta t + \delta\mathbf{X} \quad , \tag{2.2}$$

with $\mathbf{U}\delta t$ representing the mean displacement over the interval δt and $\delta\mathbf{X}$ a stochastic increment with zero mean and (as we shall see) a variance order δt. Alternatively, the random flight model predicts the displacement as the integral of the velocity, and the stochastic term acts as an acceleration:

$$\begin{aligned} \mathbf{X}(t+\delta t) &= \mathbf{X}(t) + \mathbf{U}(t)\delta t \\ \mathbf{U}(t+\delta t) &= \mathbf{U}(t) + \mathbf{A}(t)\delta t + \delta\mathbf{U} \quad , \end{aligned} \tag{2.3}$$

To see how the same math applies to a structured population model, consider a case in which organisms at different life stages are characterized by different weights. The weight of an individual will satisfy an equation such as

$$W(t+\delta t) = W(t) + g(W(t),t)\delta t + \delta W \quad , \tag{2.4}$$

where the mean rate of weight gain $[g(W(t),t)]$ depends on the current weight and perhaps on environmental conditions represented as an explicit variation in time. A specific individual will gain weight at a rate which differs from the mean in a stochastic way, depending on its success or failure at gathering the needed resources. The stochastic term, δW, may depend on the weight and environment as well.

Figure 2.1 shows examples of these three situations; each plot traces the characteristics of multiple individuals starting from the same conditions. The variability proves significant for many reasons:

- Our expectations of where we might find organisms can be quite different; the place where the probability is highest is not necessarily predicted by the mean position.
- The mean trajectory can be different from that predicted by the deterministic parts of the equation.
- The average rates of biological processes such as the consumption of resources can be altered. If, for example, the grazing rate depends nonlinearly on the weight with higher weight organisms feeding more effectively,

$$grazing = \alpha W + \beta W^2 \quad ,$$

the mean grazing rate becomes

$$\langle grazing \rangle = \alpha \langle W \rangle + \beta \langle W \rangle^2 + \beta \langle (W - \langle W \rangle)^2 \rangle$$

which is larger than that predicted from the mean weight $\langle W \rangle$ alone. Since nonlinear biological reaction terms are the norm, rather than the exception, we must expect variability to play a role in the mean dynamics; the degree of its significance remains an open question.

The individual dynamics above can be represented in general as

$$Z_i(t + \delta t) = Z_i(t) + U_i(\mathbf{Z}, t)\delta t + \delta Z_i'(\mathbf{Z}, t) \tag{2.5}$$

where $Z_1,\ Z_2,\ Z_3, \ldots Z_N$ are the variables determining the state (e.g., $\mathbf{X}$, $\mathbf{U}$, and W for weight-dependent random flight behavior). The random increments $\delta Z_i'$ have $\langle \delta Z_i' \rangle = 0$ and (as we shall see) $\langle \delta Z_i' \delta Z_j' \rangle = 2\mathcal{K}_{ij}\delta t$. For some of the equations, the random term may be absent (or, equivalently, have zero variance). Note that we could work with biased random processes without explicitly separating the mean

$$Z_i(t + \delta t) = Z_i(t) + \delta Z_i(\mathbf{Z}, t) \quad .$$

For this form, $\langle \delta Z_i \rangle = U_i \delta t$ and $\langle \delta Z_i \delta Z_j \rangle = U_i U_j \delta t^2 + 2\mathcal{K}_{ij}\delta t$. Such equations have been analyzed in detail in many places (beginning with the theory of Brownian motion, Einstein, 19xx, Wax, 19xx) and applied to many types of organisms (c.f. Okubo, 19xx, Flierl, *et al.*, 19xx); we shall adopt a simpler version (c.f. xxx) which results in much the same answer but is mathematically more straightforward.

2.3 — Random hops:

To start with a methematically and conceptually simple case, we consider motion on a discrete, one-dimensional lattice of points for the case where the mean has not been removed. During a time interval δt, an organism at lattice point x can move an integral number of lattice points $j\delta x$ with probability $\mathcal{P}_T(j\delta x|x)$.

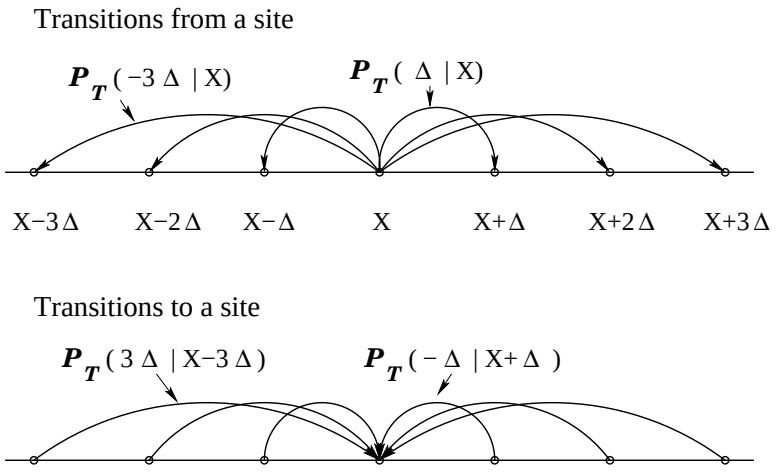

In this model, "behavior" simply means that the probability of making a hop in any particular direction depends on environmental cues at the current position x. For example, an organism may decrease the probability of moving if the food concentration is high. Or, if it can perceive gradients, it may preferentially hop to the right if the conditions seem better in that direction.

Simulating the random hop on a lattice process is easy (but somewhat more difficult than coding 2.2): at each step, a random integer conforming to the appropriate probability distribution is computed for each organism, which is then moved to the new lattice point. Experiments with only hops of $-\delta x$, 0, and δx having non-zero probabilities (figures 2.2-2.5) show:

- Peaks spread out with the rate of spread proportional to the $j \neq 0$ hop probabilities.

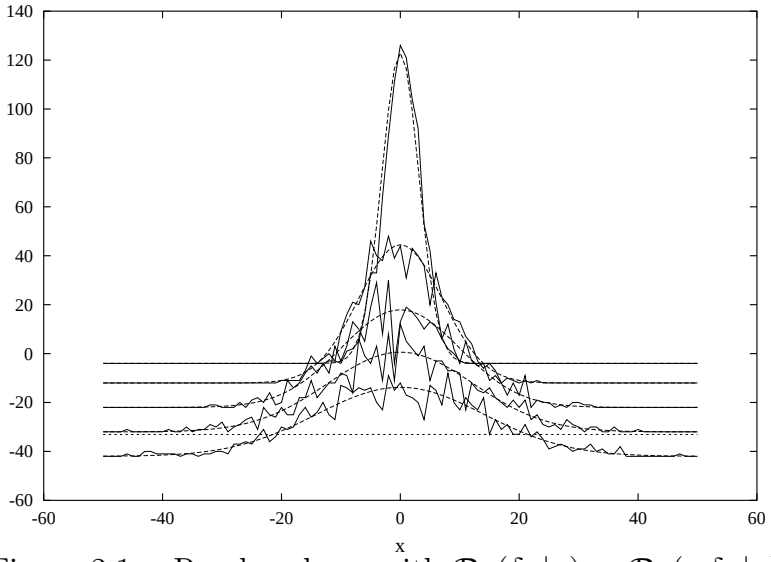

Figure 2.1a: Random hops with $\mathcal{P}_T(\delta x|x) = \mathcal{P}_T(-\delta x|x) = 0.1$, $\delta t = 1$, $\delta x = 1$. The solid line shows one realization; the dashed lines the probability distribution computed from 2.xx. Times are 50, 250, 500, 750, and 1000. Plots for successive times are displaced downwards.

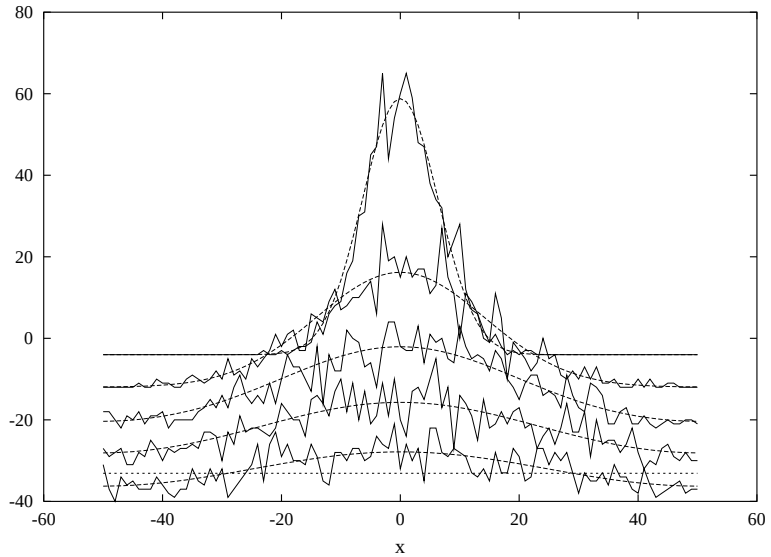

Figure 2.1b: $\mathcal{P}_T(\delta x|x) = \mathcal{P}_T(-\delta x|x) = 0.4$.

- If $\mathcal{P}_T(\delta x|x) > \mathcal{P}_T(-\delta x|x)$, the group also drifts to the right.

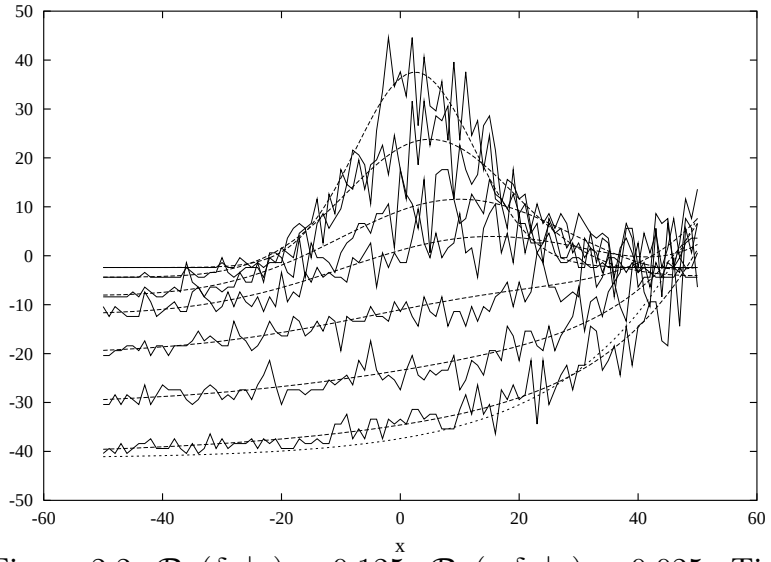

Figure 2.2: $\mathcal{P}_T(\delta x|x) = 0.125,\ \mathcal{P}_T(-\delta x|x) = 0.025$. Times are 500, 1000, 4000, 8000, 12000, 16000, and 20000. The dotted line shows the predicted steady state from the eigenvector of $\mathbf{T}$ (see below).

- If the probabilities depend on position, we see aggregation behavior. The simplest case is the isotropic one $\mathcal{P}_T(\delta x|x) = \mathcal{P}_T(-\delta x|x) = p_0 + p_1 x^2$. The organisms only change their behavior based on local conditions and do not sense gradients, yet are still able to aggregate. If the reduction in the tendency to move occurs in regions where the environment is favorable (abundant food, for example) this movement pattern (called "kinesis") will lead to enhanced growth.

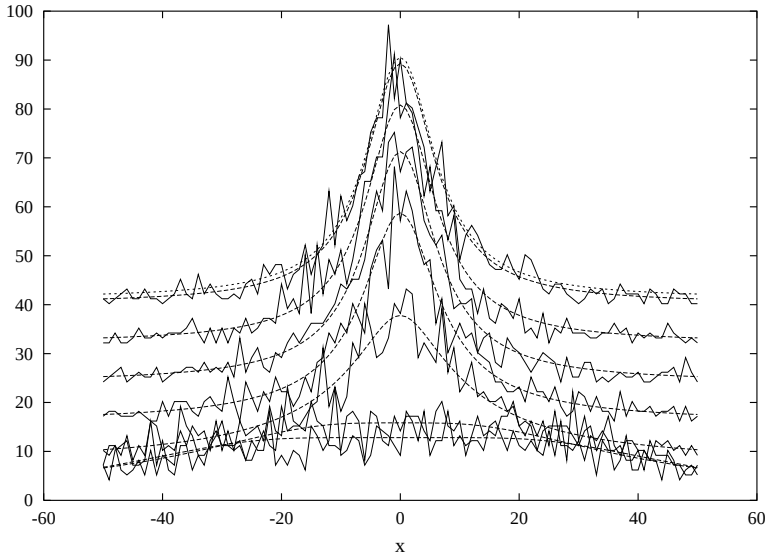

Figure 2.3: $\mathcal{P}_T(\pm\delta x|x) = 0.4(0.02 + x^2/50^2)$. Times are 500, 1000, 4000, 8000, 12000, 16000, 20000. (Plots are displaced upwards).

- If $\mathcal{P}_T(\delta x|x) - \mathcal{P}_T(-\delta x|x)$ varies with x, we can also find aggregation near the point where a decreasing $\mathcal{P}_T(\delta x|x)$ crosses an increasing $\mathcal{P}_T(-\delta x|x)$ (if such exists). This kind of behavior, called "taxis," provides another, more active aggregation mechanism for organisms which can sense conditions for some distance around them and can make directional decisions.

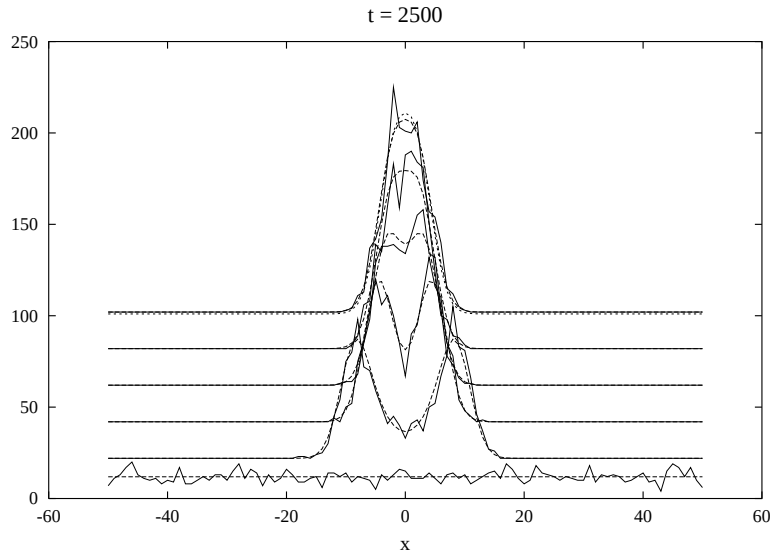

Figure 2.4: $\mathcal{P}_T(\delta x|x) = 0.4(0.02 + x^2/50^2)$ for $x < 0$ and 0.02 for $x \geq 0$. $\mathcal{P}_T(-\delta x|x) = \mathcal{P}_T(\delta x, -x)$ is the mirror image. Times are 0, 500, 1000, 1500, 2000, 2500.

Thus this very simple model can exhibit mean drifts, dispersion, and the basic mechanisms for aggregation induced by behavior (as contrasted with that generated by population dynamics).

2.3.1 — Probabilities

In addition to direct simulations of the stochastic process, we can look at how the probability $\mathcal{P}(x,t)$ of being at location x changes with time. In the 1-D case, the chance of an organism being at a particular site at time $t + \delta t$ is given by the probability that it was at a site $x - j\delta x$ at time t and made a hop of distance $j\delta x$ (summed over all j values). [The likelihood of staying at x is just $\mathcal{P}_T(0|x)$.] Therefore, the probabilities of occupying a site change according to

$$\mathcal{P}(x, t + \delta t) = \sum_j \mathcal{P}_T(j\delta x|x - j\delta x)\mathcal{P}(x - j\delta x, t) \quad . \tag{2.6}$$

Since each organism must end up somewhere, the transition probabilities are constrained by

$$\sum_j \mathcal{P}_T(j\delta x|x) = 1 \quad . \tag{2.7}$$

Not only is this procedure easy to code, it is amenable to analysis. For example, we can find the steady states, if they exist, by considering the equation for the probability written as a transition matrix

$$\vec{\mathcal{P}}(t+\delta t) = \mathbf{T}\vec{\mathcal{P}}(t)$$

with the i^{th} component of $\vec{\mathcal{P}}$ being the probability of occupying site $i\delta x$ and $T_{ij} = \mathcal{P}_T([i-j]\delta x|j\delta x)$. The steady state is just the eigenvector of $\mathbf{T}$ corresponding to the eigenvalue 1. We know that 1 is indeed an eigenvector because $(1,1,1\ldots1)\times\mathbf{T} = (1,1,1\ldots1)$ by (xx). Therefore we have a left eigenvector with eigenvalue one and must also have a corresponding right eigenvector, Figures 2.xx also show the steady states corresponding to the examples above. Note that these are calculated for a bounded domain (with the conditions on $\mathcal{P}_T$ ensuring that the organisms do not cross the edges of the area); in many cases, the probability of occupying the favorable region is inversely proportional to the domain size. We will discuss the existence and characteristics of steady solutions in more detail below.

2.3.2 — Differential Equation Version:

If we Taylor-expand 2.xx to order δt, δx, and δx^2, we find

$$\mathcal{P}(x,t) + \frac{\partial \mathcal{P}(x,t)}{\partial t}\delta t = \sum \mathcal{P}_T(j\delta x|x)\mathcal{P}(x,t) - \frac{\partial}{\partial x}\left[\sum j\delta x \mathcal{P}_T(j\delta x|x)\mathcal{P}(x,t)\right]$$

$$+\frac{1}{2}\frac{\partial^2}{\partial x^2}\left[\sum j^2\delta x^2 \mathcal{P}_T(j\delta x|x)\mathcal{P}(x,t)\right]$$

or

$$\frac{\partial \mathcal{P}(x,t)}{\partial t}\delta t = -\frac{\partial}{\partial x}\left[\mathcal{P}(x,t)\sum j\delta x \mathcal{P}_T(j\delta x|x)\right] + \frac{1}{2}\frac{\partial^2}{\partial x^2}\left[\mathcal{P}(x,t)\sum j^2\delta x^2 \mathcal{P}_T(j\delta x|x)\right]$$

The assumption here is that the scales over which the transition probabilities and $\mathcal{P}$ itself vary are much larger than the hop size δx; such an approximation – that the mean free path is short compared to scales of variability – is an intrinsic step in deriving diffusion equations.

We can define the mean velocity

$$U = \frac{1}{\delta t}\left[\sum j\delta x \mathcal{P}_T(j\delta x|x)\right] = \frac{\langle \Delta x\rangle}{\delta t}$$

and the dispersion coefficient

$$\mathcal{K} = \frac{1}{2\delta t}\left[\sum j^2\delta x^2 \mathcal{P}_T(j\delta x|x)\right] = \frac{\langle \Delta x^2\rangle}{2\delta t}$$

where $\langle \Delta x \rangle$ is the mean hop and $\langle \Delta x^2 \rangle$ is (to the appropriate order in δt the expected variance.† These definitions yield

$$\frac{\partial \mathcal{P}}{\partial t} = -\frac{\partial}{\partial x}\left[U(x)\mathcal{P}(x,t)\right] + \frac{\partial^2}{\partial x^2}\left[\mathcal{K}(x)\mathcal{P}(x,t)\right]$$

or, in standard advection-diffusion form,

$$\frac{\partial}{\partial t}\mathcal{P} = -\nabla \cdot \left[\mathbf{u}_{bio}\mathcal{P} - \kappa_{bio}\nabla\mathcal{P}\right] \tag{2.8}$$

with

$$\mathbf{u}_{bio} = \mathbf{U} - \nabla\mathcal{K} \quad , \quad \kappa_{bio} = \mathcal{K} \ .$$

We shall use this standard form (extended in 2.xx to two and three dimensions under the assumption that $\mathcal{K}$ is isotropic); keep in mind that the biological velocity includes contributions from both taxis (U) and kinesis ($-\nabla\mathcal{K}$).

Equation (2.xx) illustrates the transition from individual behavior (summarized by the quantities U and $\mathcal{K}$) to a continuum equation for changes is the density $\rho = N\mathcal{P}'$, where N is the number of organisms, and $\mathcal{P}' = \mathcal{P}/\delta x$ is a probability density (so that $\mathcal{P}'\delta x$ is the probability of being in the interval $x - \delta x/2$ to $x + \delta x/2$). Therefore the expected density satisfies the same equation as $\mathcal{P}$

$$\frac{\partial}{\partial t}\rho = -\nabla \cdot \left[\mathbf{u}_{bio}\rho - \kappa_{bio}\nabla\rho\,\right] \tag{2.9}$$

As we shall see, the same form will arise for the random flight model, but requires further approximations. As discussed in chapter xx, continuum models such as this are the most common approach to biological modelling; however, we should note that individual-based and continuum simulations can differ in a number of ways. First, of course, any particular realization will necessarily give a density distribution (calculated by summing the number of individuals in suitably sized volumes) which differs from $N\mathcal{P}'$; we would need to compute a large ensemble of realizations and average them to recover the predicted probability distribution.

Aggregation

We can see what is required for aggregation by repeating the derivation (x.x) using $\mathcal{P}$ and the appropriate velocities and diffusivities

$$\frac{\partial}{\partial t}\iint_A \mathcal{P} = -\mathcal{P}_{\partial A}\iint_A \nabla \cdot \mathbf{u}_{bio} + \oint_{\partial A} \kappa_{bio}\hat{\mathbf{n}} \cdot \nabla\mathcal{P}$$

Local maximum can be intensified only if the biological velocity (including both bias in the hops and gradients in the hop probabilities) is convergent. When the hops are restricted to a single lattice distance, we need either

$$\frac{\partial}{\partial x}\left[\mathcal{P}_T(\delta x|x) - \mathcal{P}_T(-\delta x|x)\right] < 0 \quad \text{or} \quad \frac{\partial^2}{\partial x^2}\left[\mathcal{P}_T(\delta x|x) + \mathcal{P}_T(-\delta x|x)\right] > 0$$

or both – $\mathbf{U}$ must be convergent or $\mathcal{K}$ must have a minimum.

† I.e., $\mathcal{K} = var(\Delta x)/2\delta t + U^2\delta t/2$; if the first term has a finite limit as $\delta t \to 0$, then the second term will be vanishingly small in comparison.

2.3.3 — Generalization to multiple dimensions

Now let us generalize to the full problem (2.5) where there can be a large set of state variables $\mathbf{Z}$ for each individual, including position, velocity, weight, etc.; following the same steps starting from

$$\mathcal{P}(\mathbf{z}, t+\delta t) = \sum \mathcal{P}_T(\delta\mathbf{z}|\mathbf{z}-\delta\mathbf{z})\mathcal{P}(\mathbf{z}-\delta\mathbf{z}, t)$$

(with the sum over all possible vector displacements $\delta\mathbf{z}$) and expanding, we obtain the Fokker-Planck equation

$$\frac{\partial}{\partial t}\mathcal{P} = -\frac{\partial}{\partial z_m}(U_m\mathcal{P}) + \frac{\partial^2}{\partial z_m \partial z_n}(\mathcal{K}_{mn}\mathcal{P}) \tag{2.10}$$

with $U_i = \langle\Delta z_i\rangle/\delta t$ giving the mean motion in phase space and $\mathcal{K}_{mn} = \langle\Delta z_m \Delta z_n\rangle/2\delta t$ giving the diffusion induced by the stochastic variability.

Note that the step of passing from a difference to a derivative in $\mathbf{z}$ requires the lattice size to become very small, and, concomitantly, the random terms to have a range of values, with a pattern such that the moments become independent of the mesh spacing. Thus we obtain the same equation if we begin from the equations (2.xx) and treat $\delta\mathbf{Z}'$ as a random variable with a continuous range of values (eg., Flierl, *et al.*, 19xx).†

Divergence of phase-space velocities

In chapter one, we looked briefly at the question of when mean motion results in divergence form like 2.xx versus a $U_i\frac{\partial}{\partial x_i}$ form; because $\mathcal{P}(\mathbf{z}, t)dz_1 dz_2 \ldots dz_N$ gives the probability of being within a volume Πdz_i around the point z, $\mathcal{P}$ is a "per unit volume" quantity, and the divergence form is indeed appropriate. But it is pedigogically worthwhile to see exactly how this difference plays out in the case where Z represents weight. If a 100 g organism grows to 105 g in time δt and a 103 g organism becomes 107 g (with the ones in between remaining in between), the number per unit weight will go up by a factor of $(103-100)/(107-105) = 3/2$ (see figure 2.xx). More generally, if

$$\begin{aligned} Z &\to Z + U(Z,t)\delta t \\ Z + dz &\to Z + dz + U(Z+dz,t)\delta t \simeq Z + U(Z,t)\delta t + dz\left(1 + \frac{\partial U}{\partial z}\delta t\right) \quad , \end{aligned}$$

then the volume (length in 1-D) changes by

$$dz \to dz\left(1 + \frac{\partial U}{\partial z}\delta t\right) \quad .$$

† We use, throughout, the Ito calculus appropriate to the case where the characteristics of the stochastic terms are set at the beginning of the step.

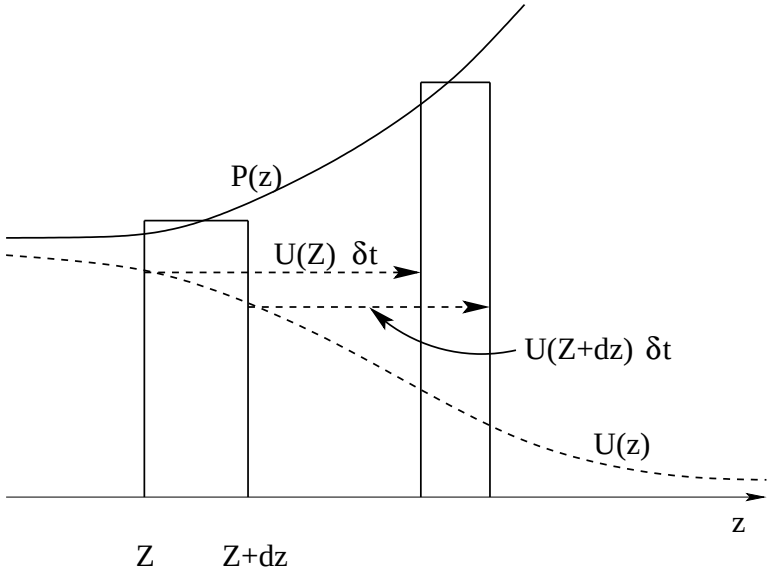

Figure 2.5: Changes in volume associated with spatially varying mean velocities $U(z,t)$

In the absence of stochastic terms, the probability satisfies

$$\begin{aligned}\mathcal{P}(z,t)dz &= \mathcal{P}(z+U(z,t)\delta t, t+\delta t)dz\left(1+\frac{\partial U}{\partial z}\delta t\right)\\ &\simeq \mathcal{P}(z,t)dz + \frac{\partial \mathcal{P}}{\partial t}\delta t dz + U\frac{\partial \mathcal{P}}{\partial z}\delta t dz + \mathcal{P}\frac{\partial U}{\partial z}\delta t dz\end{aligned}$$

so that

$$\frac{\partial \mathcal{P}}{\partial t} + U\frac{\partial \mathcal{P}}{\partial z} + \frac{\partial U}{\partial z}\mathcal{P} = \frac{\partial \mathcal{P}}{\partial t} + \frac{\partial}{\partial z}(U\mathcal{P}) = 0$$

The first two terms come from transforming movement in Lagrangian space back to Eulerian space, while the third arises from the volume changes along the trajectory.

In N dimensions, the volume of a parallelpiped defined by a set of vectors $\mathbf{v}^{(j)}$ is given by the determinant of a matrix $V_{ij} = v_i^{(j)}$ having the $\mathbf{v}$'s as its columns. If the matrix is

$$V_{ij} = dz_j \delta_{ij}$$

initially, it changes to

$$V_{ij} = dz_j\left(\delta_{ij} + \frac{\partial U_i}{\partial z_j}\delta t\right)$$

at time $t + \delta t$. The off-diagonal terms of $\mathbf{V}$ contribute to the determinant at order δt^2 or higher, so we can estimate the volume by

$$V(t+\delta t) \simeq \prod_i dz_i(1 + \frac{\partial U_i}{\partial z_i}\delta t) \simeq \left(1 + \delta t \sum_i \frac{\partial U_i}{\partial z_i}\right) \prod_i dz_i \simeq \left(1 + \delta t \sum_i \frac{\partial U_i}{\partial z_i}\right) V(t)$$

Thus the rate of change of volume is set by by the divergence (in N-dimensional space) of the velocities $V \sum_i \frac{\partial U_i}{\partial z_i}$, and the mean (determanistic) part of the evolution equation

$$\mathcal{P}(\mathbf{z}, t)V(t) = \mathcal{P}(\mathbf{z} + \mathbf{U}(\mathbf{z}, t)\delta t, t + \delta t)V(t + \delta t)$$

results in

$$\frac{\partial \mathcal{P}}{\partial t} + U_i \frac{\partial \mathcal{P}}{\partial z_i} + \mathcal{P}\frac{\partial U_i}{\partial z_i} = 0$$

(reverting to summation notation).

With this derivation providing more detail on the underpinnings of the advective part of the Fokker-Planck equation, we shall use 2.xx or its advective-diffusive form

$$\frac{\partial}{\partial t}\mathcal{P} + \frac{\partial}{\partial z_m}\left[(U_m - \frac{\partial}{\partial z_n}\mathcal{K}_{mn})\mathcal{P}\right] = \frac{\partial}{\partial z_m}\mathcal{K}_{mn}\frac{\partial}{\partial z_n}\mathcal{P} \tag{2.11}$$

in the following sections and chapters.

2.3.4 — Comparisons

We have discussed three different approaches: first, the "individual-based model" (IBM) with the positions of some number of organisms advanced by using random numbers (in the lattice problem, to see if each organism should hop left, right, or not at all; in the continuous problem to select a $\delta\mathbf{X}$ – see appendix A.2). Second, we can compute the evolution of the probability distribution using (2.xx). Thirdly, we can solve the diffusion equation (2.xx-xx). Figure 2.xx shows a comparison of the three methods after 100 time steps for the simplest problem of dispersion from a point. For the IBM, we compute the probabilities by averaging 10,000 realizations; the diffusion equation solution is computed directly from the analytic solution

$$\mathcal{P}(x, t) = \frac{1}{\sqrt{4\pi\mathcal{K}t}} \exp(-x^2/4\mathcal{K}t)$$

The IBM simulations, which we can also think of as releasing 10,000 individuals at $x = 0$, show statistical fluctuations around the expected probabilities, most noticeably at the tails where the numbers are small so that the fluctuations are relatively large. Note also that the maximum distance traveled by any of the organisms was less than 20% of the potential maximum distance ($100\delta x/\delta t$ units).

The direct calculation of $\mathcal{P}$ from 2.xx likewise has a cutoff for $|x| > 100$, which correponds to all 100 hops being to the left or to the right; the organisms spread at a finite rate of speed bounded by $u_{max} = \delta x/\delta t$. The diffusion equation, in contrast, gives a

finite, albeit tiny, chance of being much farther away, but underestimates the probability of being in the range (0.5–1)$\times u_{max}t$.

We can think of problems where this difference could become significant: if an organism is trying to maintain itself against advective losses in a favorable area (see xx.xx), its maximum movement speed could be critical in determining whether it can diffuse back and reseed a growing population.

For this very simple problem, the diffusion equation works well as long as the regions with a small number of organisms (or very low probabilities) are not of significant concern. If that is not true, a probabilistic model or an IBM would be called for (with the recognition that individual realizations may turn out quite differently from each other). We shall return to the advantages of each approach when we couple movement and physical flows.

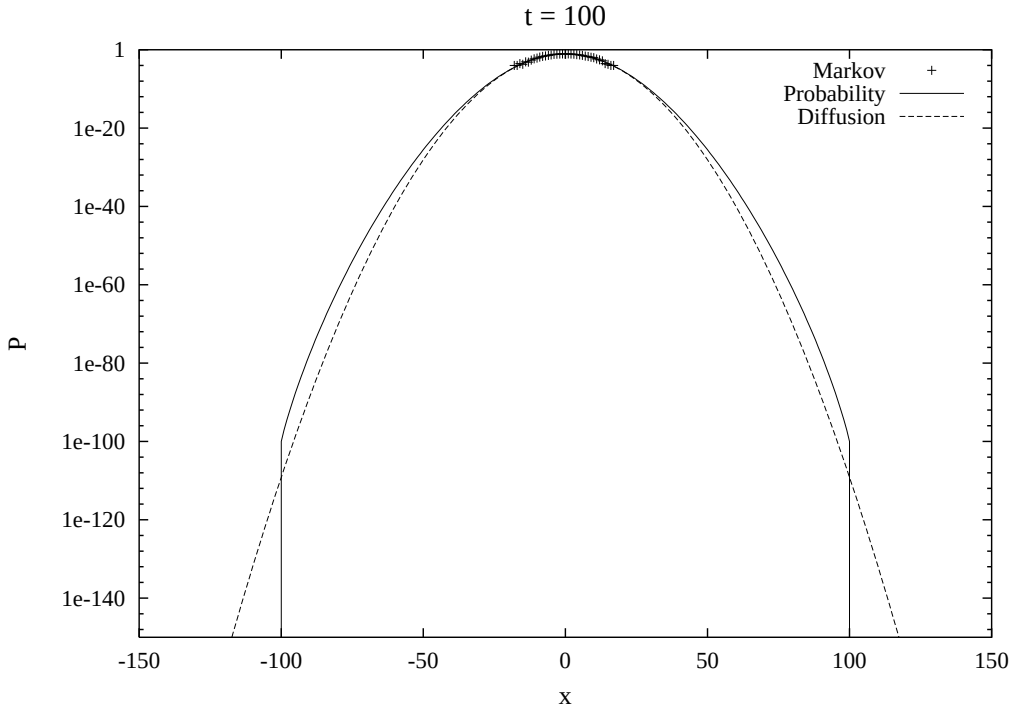

Figure 2.6a: Probability of being at position x at $t = 100$ for an organism released at $x = 0$ at time 0. The parameters are $\mathcal{P}_l = \mathcal{P}_r = 0.1$ and $\delta x = \delta t = 1$.

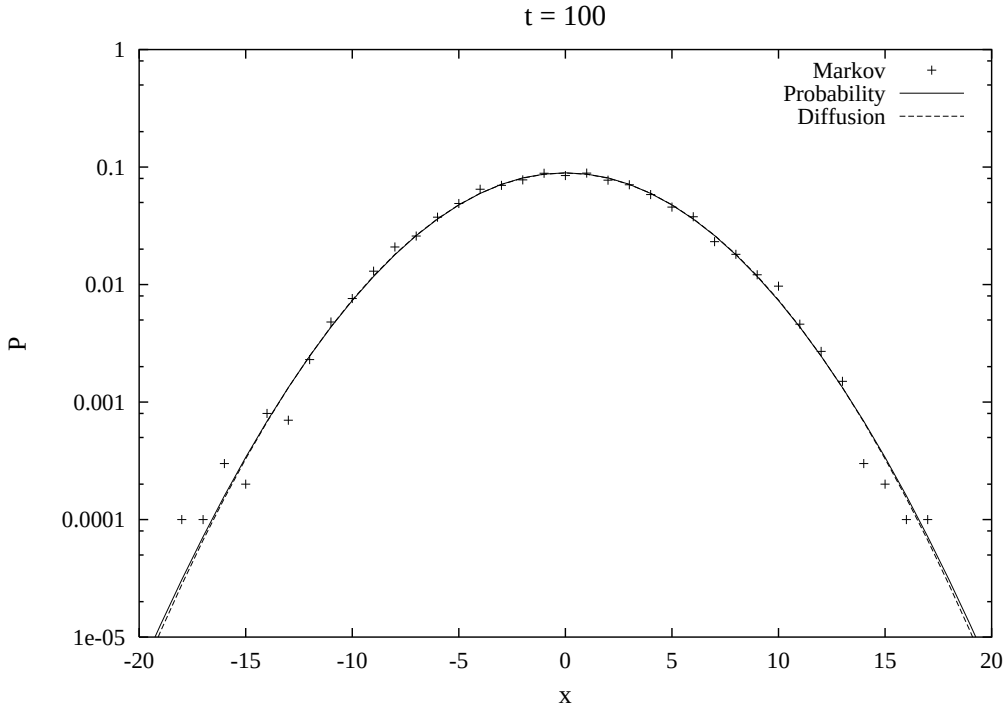

Figure 2.7b: Closeup of previous figure.

2.4 — Random flight – Lattice-Boltzmann model

While "hop" might be an apt description of escape responses, many organisms move by swimming, so that a random flight model seems like a more appropriate model for their motion. Taking the positions and velocities as control variables, with mean accelerations $\mathbf{a}$ and stochastic velocity changes $\delta\mathbf{U}$, we can find a version of the Boltzmann equation directly:

$$\frac{\partial}{\partial t}\mathcal{P}(\mathbf{x},\mathbf{u},t) = -\frac{\partial}{\partial x_i}(u_i\mathcal{P}) - \frac{\partial}{\partial u_i}(a_i\mathcal{P}) + \frac{\partial}{\partial u_i}\frac{\partial}{\partial u_j}(\mathcal{K}_{ij}\mathcal{P}) \tag{2.12}$$

with $\mathcal{K}_{ij} = \frac{1}{2}\langle\delta U_i \delta U_j\rangle/\delta t$. As before, the stochastic terms induce a diffusion in the relevant space; in this case, the velocity dimension. We can regard (2.xx) as a differential form of the Boltzmann equation, although (unlike the gas dynamics case he considered originally) the equation is linear. However, social behavior (responses such as attraction to congeners) leads to expected values of δu or δu^2 which depend on the density (related to $N\mathcal{P}$) so that the equation can once again become nonlinear.

We will see that, under some restrictions, the random flight model again leads to an advection-diffusion equation for the density of N organims

$$\rho(\mathbf{x},t) = N\int d\mathbf{u}\,\mathcal{P}(\mathbf{x},\mathbf{u},t) \quad .$$

For illustriative purposes, a simple 1D version can help us understand the limits of validity of the diffusion approximation. This model constrains the velocities to be $-u$, 0, $+u$. We can then solve for the probability changes in a two-step process:

1) Translation

$$\begin{aligned}\mathcal{P}(x,-u,t+\delta t^-) &= \mathcal{P}(x+u\delta t,-u,t)\\ \mathcal{P}(x,0,t+\delta t^-) &= \mathcal{P}(x,0,t)\\ \mathcal{P}(x,+u,t+\delta t^-) &= \mathcal{P}(x-u\delta t,+u,t)\end{aligned}$$

which can be written as

$$\mathcal{P}(x,u_i,t+\delta t^-) = \mathcal{P}(x-u_i\delta t,u_i,t)$$

2) Acceleration

$$\mathcal{P}(x,u_i,t+\delta t) = \sum_j \mathcal{P}_T(u_i-u_j|x,u_j,t)\mathcal{P}(x,u_j,t+\delta t^-)$$

where $\mathcal{P}_T(\delta u|x,u_j,t)$ is the probability of accelerating by δu given the current location x and velocity u_j.

Combining these gives the probability evolution equation

$$\mathcal{P}(x,u_i,t+\delta t) = \sum_j \mathcal{P}_T(u_i-u_j|x,u_j,t)\mathcal{P}(x-u_j\delta t,u_j,t) \tag{2.13}$$

In essense, this is a discrete form of an integro-difference equation (c.f. Neubert, 19xx)

To move towards a differential equation version, we can rewrite this is a form convenient for Taylor-expanding: since the columns of the transition matrix must sum to one

$$\sum_i \mathcal{P}_T(\delta u_i|x,u_j,t) = 1$$

[the final velocity must be one of the set of possible velocities], we can subtract the identity matrix off explicitly

$$\begin{aligned}\mathcal{P}(x,u_i,t+\delta t) - \mathcal{P}(x-u_i\delta t,u_i,t) &= \sum_j \left[\mathcal{P}_T(u_i-u_j|x,u_j,t) - \delta_{ij}\right]\mathcal{P}(x-u_j\delta t,u_j,t) \\ &\equiv \delta t \sum_j \mathcal{T}(u_i-u_j|x,u_j,t)\mathcal{P}(x-u_j\delta t,u_j,t)\end{aligned}$$

with the turning rate matrix satisfying $\sum_i \mathcal{T}(u_i-u_j|x,u_j,t) = 0$. The resulting differential equation system

$$\frac{\partial}{\partial t}\mathcal{P}(x,u_i,t) + u_i\frac{\partial}{\partial x}\mathcal{P}(x,u_i,t) = \sum_j \mathcal{T}(u_i-u_j|x,u_j,t)\mathcal{P}(x,u_j,t)$$

will be examined for the three-state model under the assumption that the stopping [$S = \mathcal{T}(\pm u|x,\mp u,t)$] and turning rates [$T = \mathcal{T}(\pm 2u|x,\mp u,t)$] are independent of the direction of travel, but the probabilities of starting from rest [$R_+ = \mathcal{T}(u,x,0,t)$, $R_- = \mathcal{T}(-u|x,0,t)$] may be asymmetric

$$\begin{aligned}\frac{\partial}{\partial t}\mathcal{P}_- &= -\frac{\partial}{\partial x}(-u\mathcal{P}_-) - (T+S)\mathcal{P}_- + R_-\mathcal{P}_0 + T\mathcal{P}_+ \\ \frac{\partial}{\partial t}\mathcal{P}_0 &= S\mathcal{P}_- - R_-\mathcal{P}_0 - R_+\mathcal{P}_0 + S\mathcal{P}_+ \\ \frac{\partial}{\partial t}\mathcal{P}_+ &= -\frac{\partial}{\partial x}(u\mathcal{P}_+) + T\mathcal{P}_- + R_+\mathcal{P}_0 - (T+S)\mathcal{P}_+\end{aligned}$$

We can rewrite these in terms of the density $\rho = N(\mathcal{P}_- + \mathcal{P}_0 + \mathcal{P}_+)$, the momentum or mass flux $J = N(u\mathcal{P}_+ - u\mathcal{P}_-)$, and the rest density $\rho_0 = N\mathcal{P}_0$:

$$\begin{aligned}\frac{\partial}{\partial t}\rho &= -\frac{\partial}{\partial x}J \\ \frac{\partial}{\partial t}J &= -\frac{\partial}{\partial x}u^2(\rho-\rho_0) - (S+2T)J + u(R_+-R_-)\rho_0 \\ \frac{\partial}{\partial t}\rho_0 &= S\rho - (S+R_-+R_+)\rho_0\end{aligned} \tag{2.14}$$

Diffusion Approximation

The three equations 2.xx (or the original form 2.xx) predict a diffusive-like spreading of an initial condition (see figure 2.xx), although once again the behavior is different near the leading edges of the spreading patch. The key to approximating these 2.xx as a diffusion equation lies in the fact that the behavioral rates (S, $R_\pm$, and T) do not appear in the equation for the density. If the transition rates are fast, we can solve the second and third equations by assuming that ρ is quasi-steady, so that the rest density and the flux rapidly approach the values

$$\rho_0 \simeq \frac{S}{S + R_- + R_+)}\rho$$

and

$$J \simeq \frac{u(R_+ - R_-)S}{(S + 2T)(S + R_- + R_+)}\rho - \frac{u^2}{S + 2T}\frac{\partial}{\partial x}\left(\frac{R_- + R_+}{S + R_- + R_+}\rho\right)$$

or

$$J = \mathbf{u}_{bio}\rho - \kappa_{bio}\nabla\rho$$

with

$$u_{bio} = \frac{u(R_+ - R_-)S}{(S + 2T)(S + R_- + R_+)} - \frac{u^2}{S + 2T}\frac{\partial}{\partial x}\frac{R_- + R_+}{S + R_- + R_+}$$

and

$$\kappa_{bio} = \frac{u^2(R_- + R_+)}{(S + 2T)(S + R_- + R_+)} \quad .$$

In terms of the preferred velocity U and the relaxation rate $r = S + 2T$ for the flux, we have

$$u_{bio} = U - \frac{1}{r}\nabla(r\kappa_{bio})$$

Thus the biological velocity and diffusivity from the three-state random flight model have much the same structure as the diffusivity as the random-hop model (although there is an extra factor of r).

Single Equation Version

Keller (2004) has described corrections to the random hop model which give a differential equation having finite signal propagation speeds; here, we shall see that the same applies to the three-state random flight model. We look first at the case without a resting state $\rho_0 = S = R_\pm = 0$ and take T to be constant

$$\frac{\partial}{\partial t}\rho = -\frac{\partial}{\partial x}J$$
$$\frac{\partial}{\partial t}J = -u^2\frac{\partial}{\partial x}\rho - 2TJ \quad .$$

If we eliminate J, we obtain the telegraph equation

$$\frac{\partial^2}{\partial t^2}\rho + 2T\frac{\partial}{\partial t}\rho = u^2\frac{\partial^2}{\partial x^2}\rho \quad ,$$

which has signals propagating like waves at a finite speed u. The diffusion equation is obtained by assuming $\frac{\partial}{\partial t}\rho << 2T\rho$, so that the first term can be dropped. To see where such an approximation is valid, we can substitute the spreading solution for diffusion into this inequality. The resulting requirement $x < O(\sqrt{\kappa t})$ with $\kappa = u^2/2T$ shows that we can only apply the diffusion equation for small enough distances (c.f. Keller, 2004). If the very small populations at greater distances are a significant concern, either the IBM, the probability equation (2.xx) or the PDE's (2.xx) should be used.

The three state model can likewise be reduced to a single equation when the parameters – stopping, turning, and restarting rates – are constant:

$$(\frac{\partial}{\partial t} + S + R_- + R_+)(\frac{\partial}{\partial t} + S + 2T)\frac{\partial}{\partial t}\rho = -\frac{\partial}{\partial x}\left[u(R_+ - R_-)\rho - \frac{\partial}{\partial x}u^2(\frac{\partial}{\partial t} + R_- + R_+)\rho\right]$$

Again, the diffusion equation arises from neglecting the $\frac{\partial}{\partial t}$ terms in the parentheses; the unapproximated third order equation or the third order system (2.xx) results in finite propagation speeds $\pm u$.

2.4.1 — Characteristics of the Boltzmann equation

Once the form of the mean acceleration, a_i, and the covariances of the stochastic jerks, $\mathcal{K}_{ij}$, are specified, the Boltzmann equation can predict the evolution of the joint position/velocity distribution. Velocity data for organisms in the ocean (or even in the lab) are exceedingly rare; therefore, we would like to determine the changes in density

$$b(\mathbf{x}, t) = N\int d\mathbf{u}\mathcal{P}(\mathbf{x}, \mathbf{u}, t)$$

(the number of organisms times the probability of being at $\mathbf{x}$ at time t irrespective of the velocity) without fully solving for the probability distribution. Multiplying (2.xx) by N

and integrating over the velocity shows that the density changes by a divergence of the flux of organisms:

$$\frac{\partial}{\partial t} b = -\nabla \cdot \mathbf{J} \quad , \qquad \mathbf{J}(\mathbf{x}, t) = N \int d\mathbf{u}\ \mathbf{u} \mathcal{P}(\mathbf{x}, \mathbf{u}, t)$$

Attempting to predict the components of J, however, runs into the "closure" problem: the rate of change of the first moment (in $\mathbf{u}$) of $\mathcal{P}$ requires knowledge of the second moment

$$\frac{\partial}{\partial t} J_i = -\frac{\partial}{\partial x_j} (N \int d\mathbf{u}\ u_i u_j \mathcal{P}) + N \int a_i \mathcal{P}$$

and the second moment requires the third,

$$\frac{\partial}{\partial t} (N \int d\mathbf{u}\ u_i u_j \mathcal{P}) = -\frac{\partial}{\partial x_k} (N \int d\mathbf{u}\ u_i u_j u_k \mathcal{P}) + N \int d\mathbf{u}\ \mathcal{K}_{ij} \mathcal{P} \quad ,$$

etc. Thus we cannot generally write a simple equation for the density unless we make a "closure hypothesis" which leads to some kind of approximate formula relating higher moments to lower ones. In the following section, we shall employ a very simple closure. Before that, we will explore some examples of the behavior of the full Boltzmann equation.

Suppose the deterministic acceleration $\mathbf{a}$ represent an organism's attempt to swim at a speed $\mathbf{V}(\mathbf{x}, t)$; when the velocity is perturbed away from this value by the random accelerations, it will relax back at a rate $r(\mathbf{x}, t)$

$$a_i = -r(u_i - V_i) \quad .$$

The preferred velocity, $\mathbf{V}$, has two parts: the fluid velocity $\mathbf{u}$ (i.e, we expect the drag to eliminate initial motion relative to the water) and any consistent swimming/ floating/ sinking relative to the water. We also assume that the random accelerations are isotropic and depend only on position

$$\mathcal{K}_{ij} = r^2 \kappa(\mathbf{x}, t) \delta_{ij}$$

($\mathcal{K}$, as a diffusivity in velocity space has units $L^2 T^{-3}$; the factor of r^2 gives κ ordinary diffusivity units $L^2 T^{-1}$ as well as leading to a simple form below). The Boltzmann equation

$$\frac{\partial}{\partial t} \mathcal{P} = -\frac{\partial}{\partial x_i} [u_i \mathcal{P}] + \frac{\partial}{\partial u_i} [r(u_i - V_i) \mathcal{P}] + \frac{\partial^2}{\partial u_i^2} [r^2 \kappa \mathcal{P}] \tag{2.15}$$

has a simple Gaussian solution when $\mathbf{V}$, r, and κ are constant:

$$\mathcal{P} = P_0 \mathcal{G}(\mathbf{u} - \mathbf{V} | r\kappa) \quad , \qquad \mathcal{G}(\mathbf{z}|\sigma) = (2\pi\sigma)^{-d/2} \exp(-|\mathbf{z}|^2 / 2\sigma) \quad ,$$

with d being the dimensionality of $\mathbf{z}$ and σ the variance in any direction. Figure 2.xx illustrates the way the probability distribution relaxes to this state: the "flow" ($\frac{\partial X}{\partial t}$, $\frac{\partial U}{\partial t}$) in ($x$, u) space acts like a combination of shear and convergence towards the zero velocity

axis ($\mathbf{V} = 0$ for this example). The latter is balanced by the diffusion, leading to the Gaussian distribution with velocity variance $r\kappa$.

Figure 2.xx shows how an initial state

$$\mathcal{P} = \frac{1}{2} p_0 [1 + \cos(kx)] \exp(-\beta_2 u^2)$$

relaxes to an x-independent final state with a velocity variance $r\kappa$. The solutions

$$\mathcal{P} = a_0 \exp(-c_0 u^2) + \Re[a_1 \exp(\imath b_1 u + \imath k x - c_1 u^2)]$$

$$\frac{\partial}{\partial t} a_j = -2\mathcal{K} a_j c_j - \mathcal{K} a_j b_j^2 + r a_j \quad , \quad \frac{\partial}{\partial t} b_j = -4\mathcal{K} b_j c_j + r b_j - k \quad , \quad \frac{\partial}{\partial t} c_j = 2 r c_j - 4\mathcal{K} c_j^2$$

end up in the asymptotic state $c_1 = r/2\mathcal{K}$, $b_1 = -k/r$ and $\frac{\partial}{\partial t} a_1 = -a_1 \mathcal{K} k^2 / r^2 = -\kappa k^2 a_1$. Thus spatial variability is smoothed out with an asymptotic decay rate which is identical to that predicted by a diffusion equation (figure 2.xx). But the decay rate for the Boltzmann equation deviates noticeably from the diffusion model during the initial stages. Consider first the case when the initial state has a velocity variance which is large compared to the equilibrium, and note the the period when the density variations decrease very rapidly. The process that speeds up the effective diffusion rate is analogous to "shear dispersion," treated in xx.xx.xx. The flow in the (x,u) phase space has strong north-south shear in the east-west velocity (treating the u axis as though it were north). This tilts structures over so that the distance between highs and lows decreases as different regions interleave and provides strong gradients on small scales, which the diffusion can then remove very effectively. Indeed, the tilt persists in the asymptotic decay regime, as the solution above demonstrates. The slow decay seen initially occurs because the probability distribution is only diffusing in u which has no effect on ρ; the density variations only decrease as shear dispersion sets in.

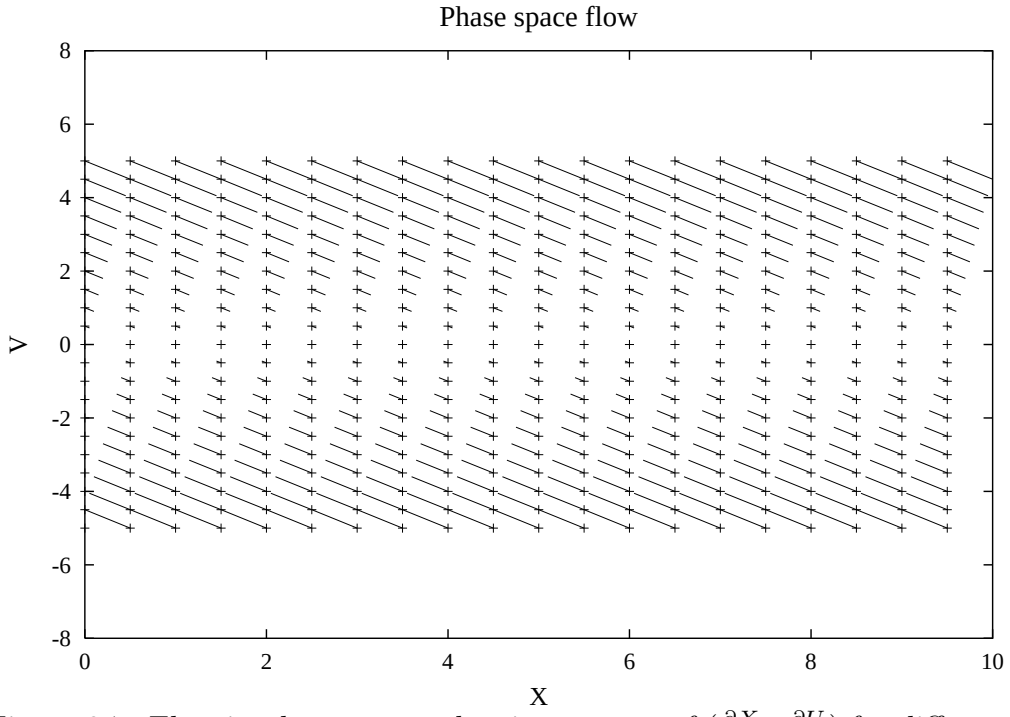

Figure 2.7: Flow in phase space, showing vectors of $(\frac{\partial X}{\partial t},\ \frac{\partial U}{\partial t})$ for different values of $(X,\ U)$.

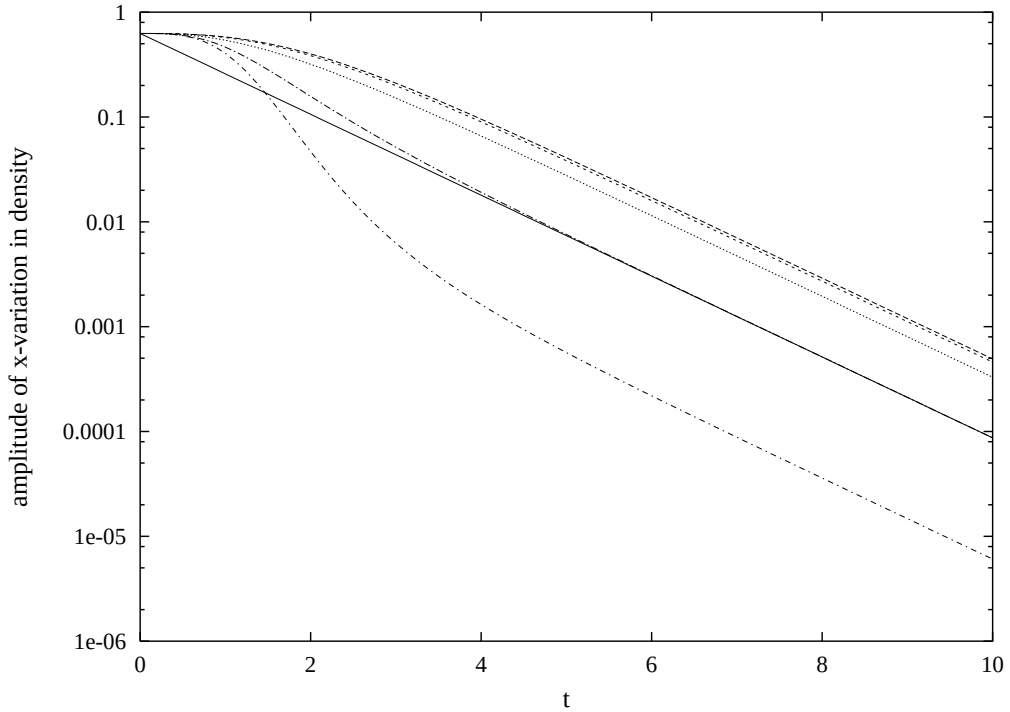

Figure 2.8: Decay of the x variable part of the field. The straight lines shows the diffusion approximation. The others (from the bottom up) are for initial widths (in velocity) of $\sqrt{10}$, 2, 1, 0.5, and $\sqrt{0.1}$ times the equilibrium width. Parameters are $r = 1$, $\kappa = 0.25$.

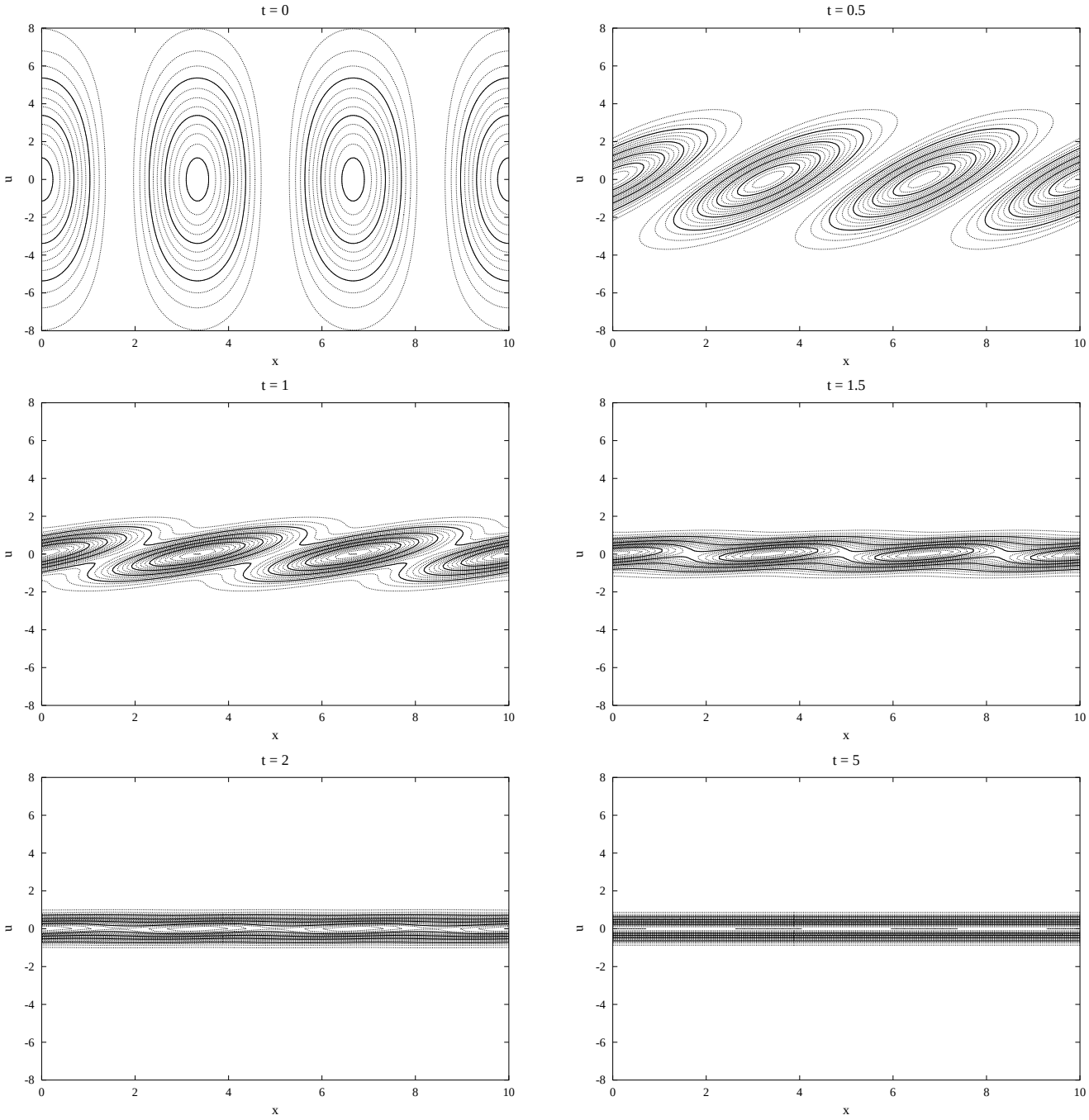

Figure 2.9: Probability distributions $\mathcal{P}(x, u, t)$ for various times. The initial condition has a velocity variance which is 10 times larger than the equilibrated variance.

The two aggregation behaviors discussed in the context of the random hop model (c.f., figures 2.xx and 2.xx) appear in the random flight model as well when $\mathbf{V}$ or $\mathcal{K}$ depend on position. Taxis (convergent $\mathbf{V}$) has a very clear signature in the (x,u) plane: the flow converges vertically to a line $V(x)$ rather than to the $u = 0$ axis. However, the flow component along this curve is non-zero, so that the trajectory will spiral in towards the point where $u = 0$ (Figure 2.xx). Hence the advective parts of the problem provide a direct tendency to accumulate at convergence points; the diffusion simply broadens the probability distribution around the center of the patch.

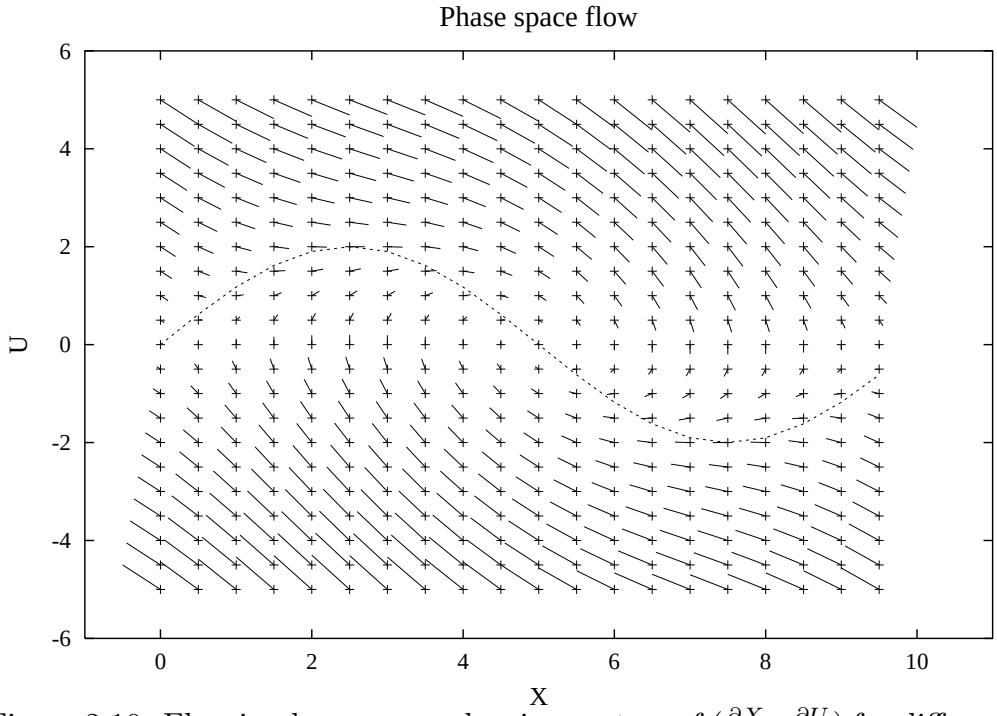

Figure 2.10: Flow in phase space, showing vectors of $(\frac{\partial X}{\partial t},\ \frac{\partial U}{\partial t})$ for different values of $(X,\ U)$. In this case, the preferred velocity is $V = 2\sin(2\pi x/10)$ as shown by the dotted line.

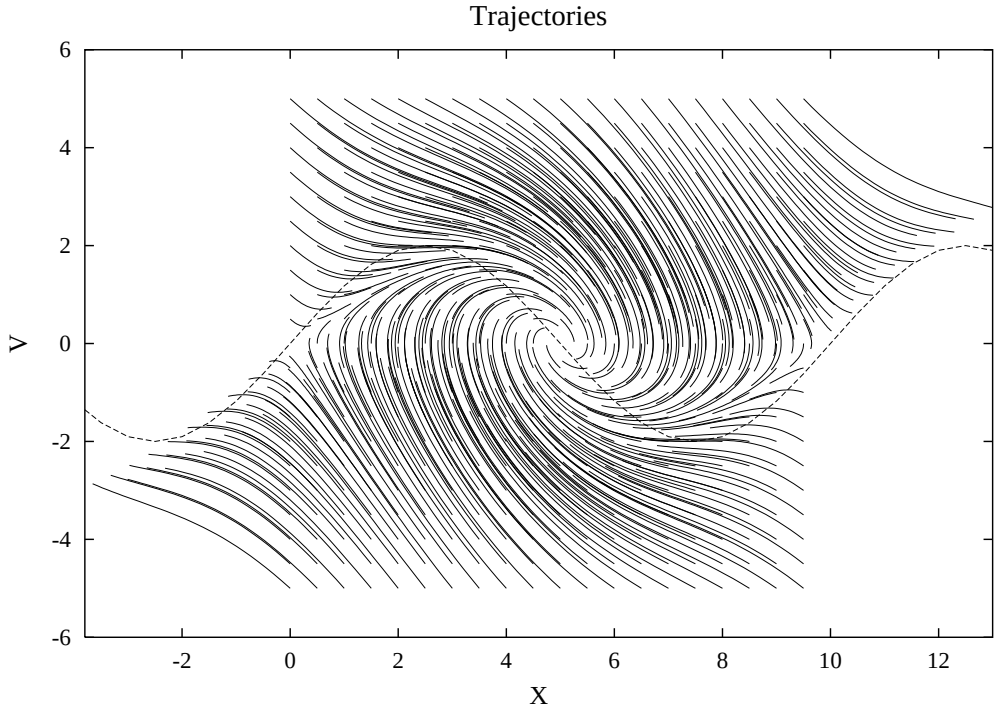

Figure 2.11: Trajectories starting from different $(X,\ U)$ points, showing the convergence towards x_0 where $V = 0$ and $\frac{\partial V}{\partial x} < 0$.

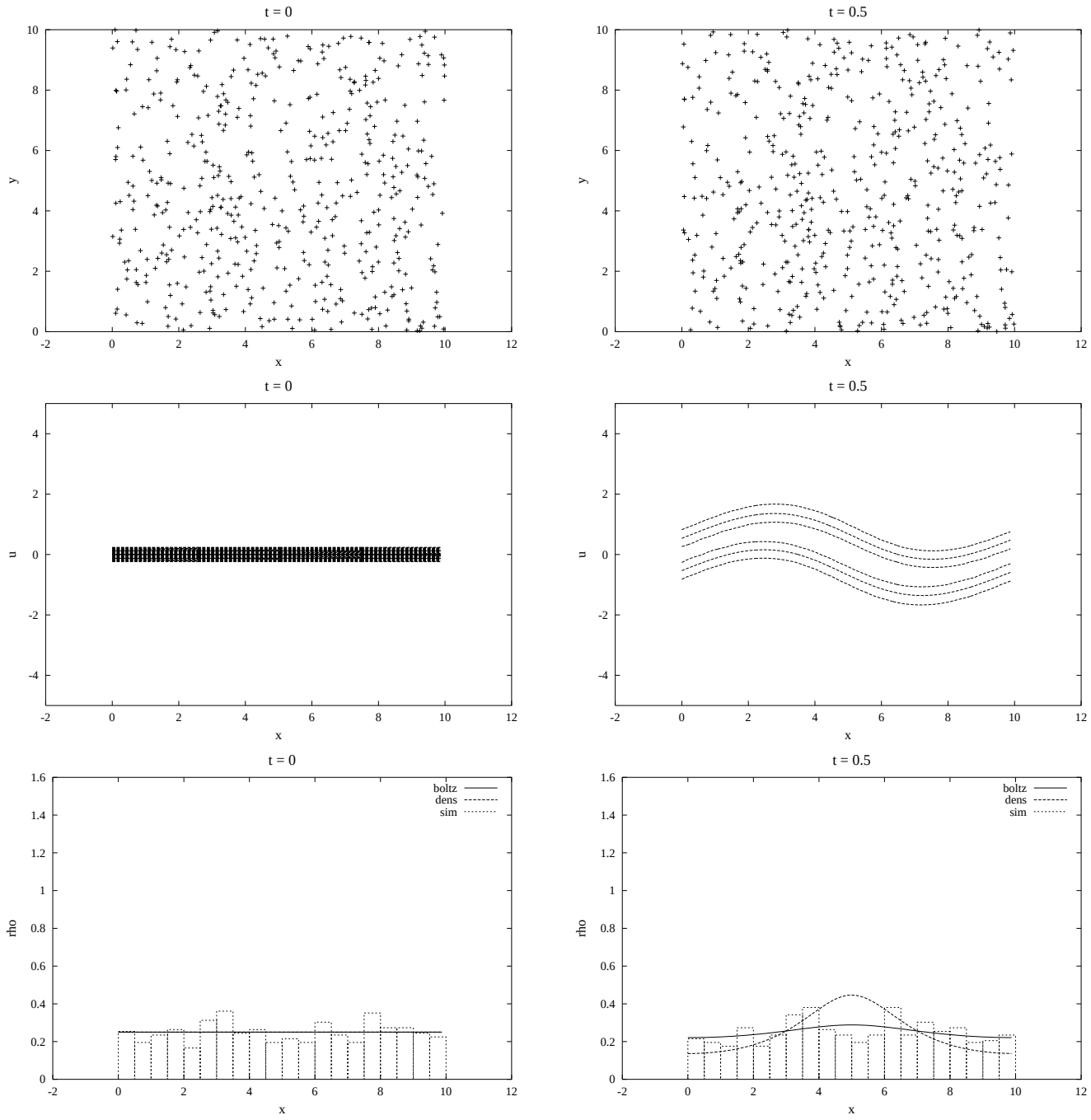

Figure 2.12a: Taxis experiments with $\mathcal{K} = 4$, $V = 2\sin(2\pi x/10)$. The upper panels show a simulation of the movement, the middle contours of $\mathcal{P}(x, u, t)$, and the lower panels show ρ from the simulation (histograms), from $\int du\mathcal{P}$ (solid) and from the density equation 2.xx (dashed). $t = 0$, 0.5.

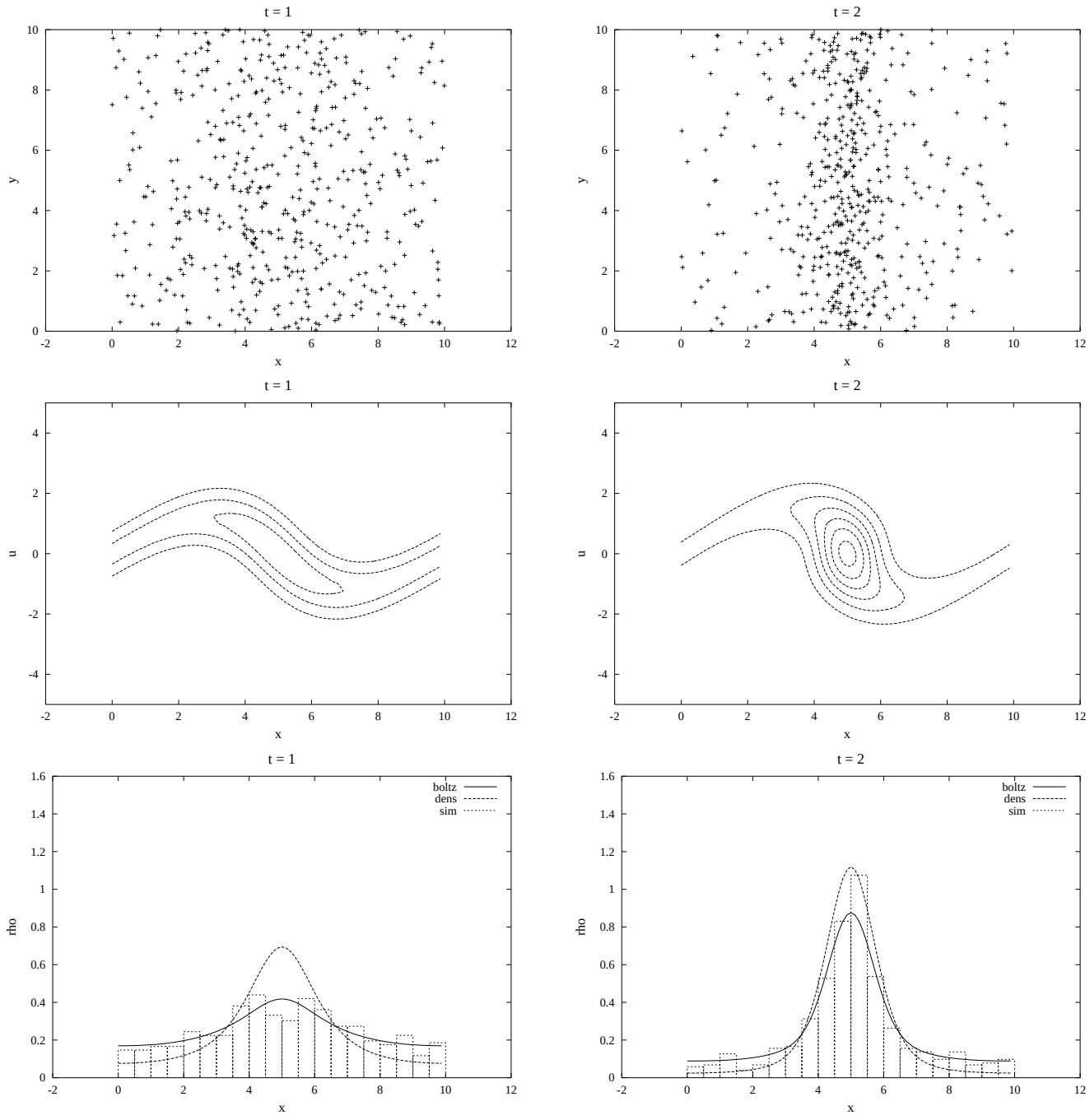

Figure 2.12b: $t = 1$, 2.

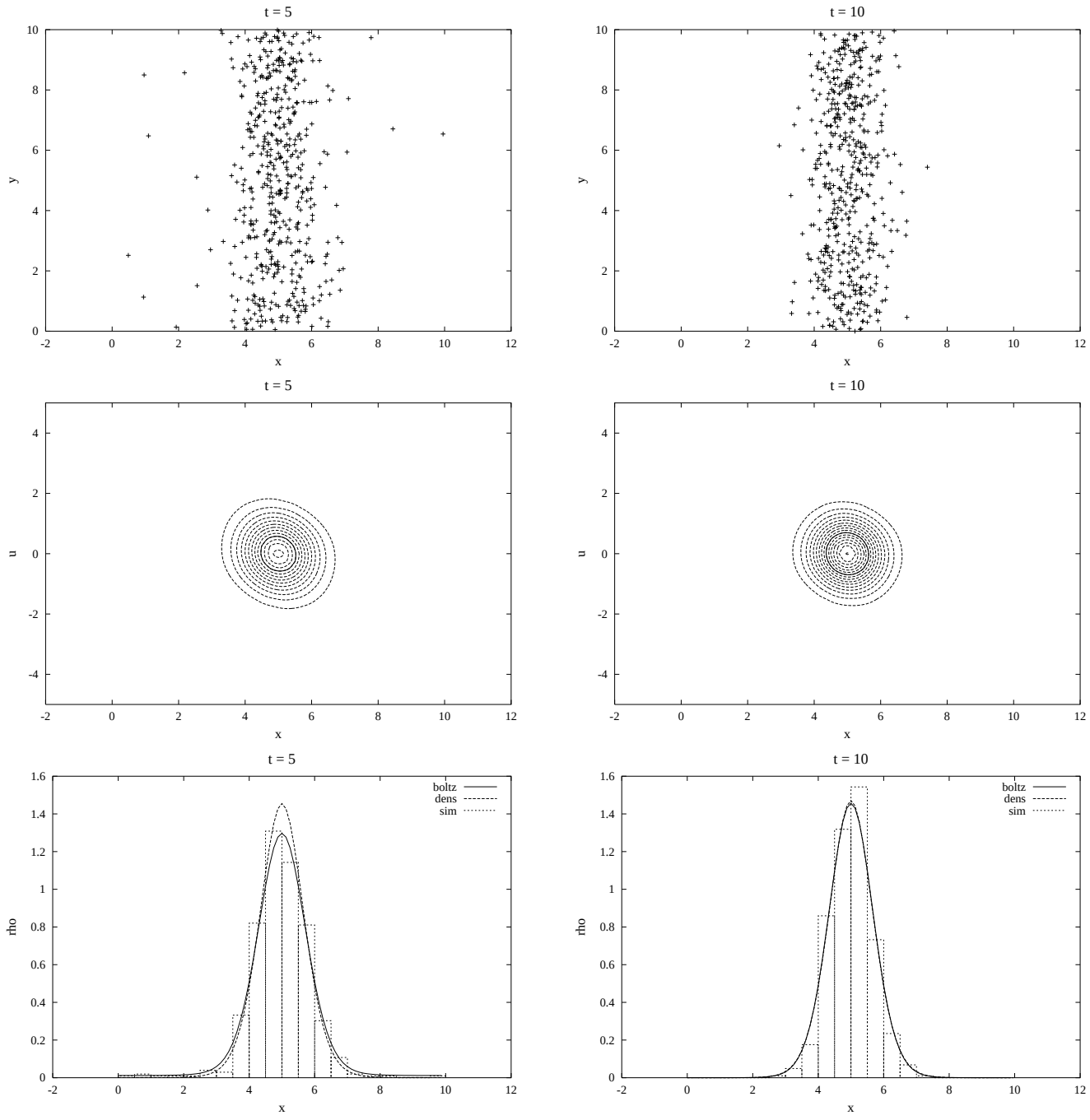

Figure 2.12c: $t = 5$, 10.

Kinesis is slightly more difficult to understand. Suppose $r\kappa$ is small in a region surrounding $x = 5$. If the initial distribution has the same structure in u at all x points (e.g., all organisms start with zero velocity), it will adjust towards a narrower distribution of velocities near $x = 0$; since the probability distribution is initially uniform in x, $\mathcal{P}(x, u, t)$ will have a higher peak at the origin. The non-uniform spreading has no direct effect on the density; however, it creates x-gradients of $\mathcal{P}$ on the north and south resulting in higher values being advected towards the $x = 5$ line and in towards $u = 0$. The distributions at times $t = 1$ and 2 show clearly the high values on the northwest side created by rightward advection of the wide distribution and the low values on the northeast side of $x = 5$. The opposite situation holds in the $u < 0$ region. As a result the flux, $J = \int du\, u\mathcal{P}$ will be positive for $x < 5$ (since the distribution of $\mathcal{P}$ is skewed towards the positive values of u) and negative for $x > 5$. Therefore the density will increase in the low $\mathcal{K}$ region.

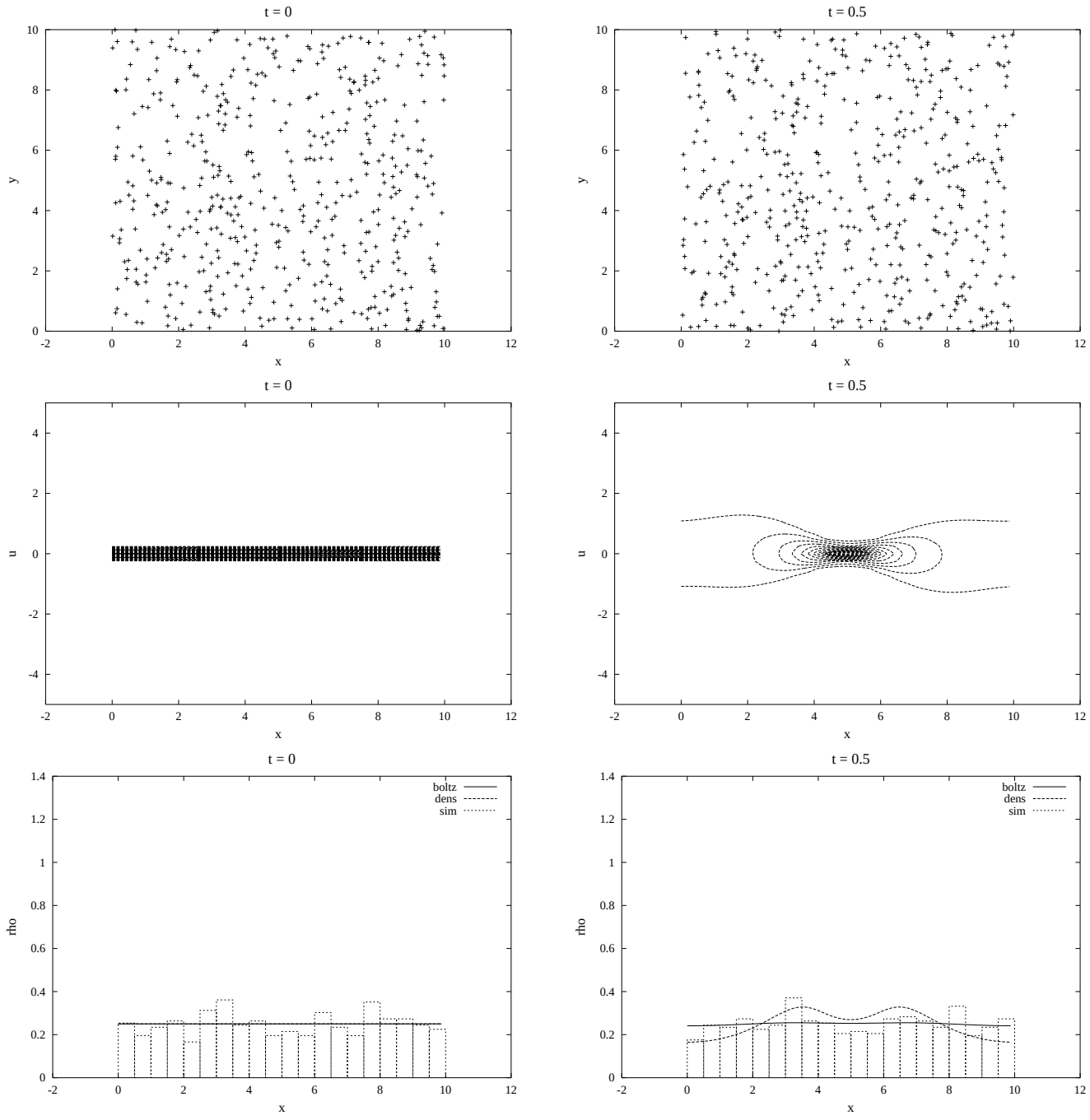

Figure 2.12a: Kinesis experiments with $\mathcal{K} = \frac{1}{2}[1.5+1.2\cos(2\pi x/10)]^2$. The upper panels show a simulation of the movement, the middle contours of $\mathcal{P}(x,u,t)$, and the lower panels show *rho* from the simulation (histograms), from $\int du\mathcal{P}$ (solid) and from the density equation 2.xx (dashed). $t = 0$, 0.5.

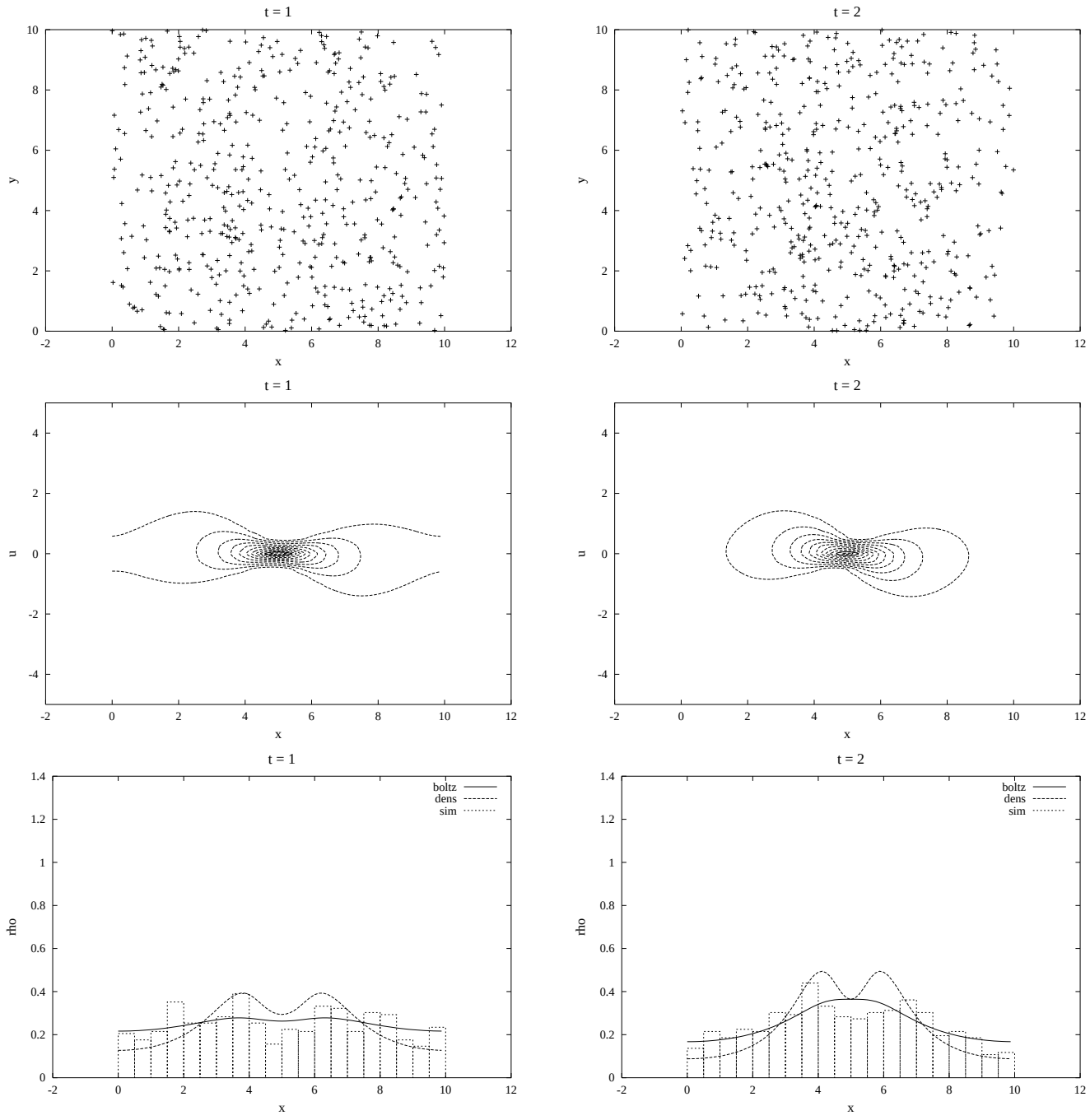

Figure 2.12b: $t = 1$, 2.

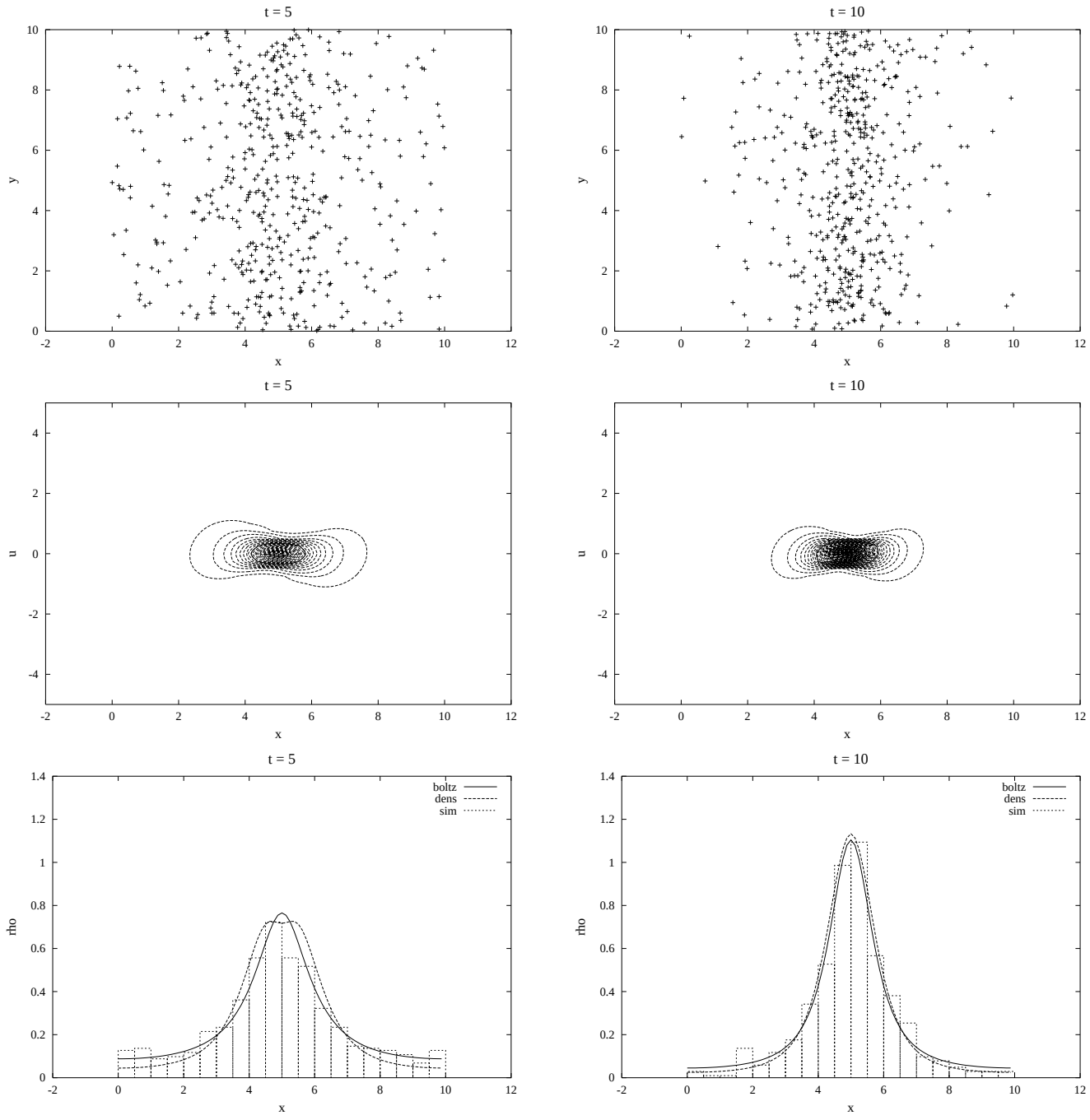

Figure 2.12c: $t = 5$, 10.

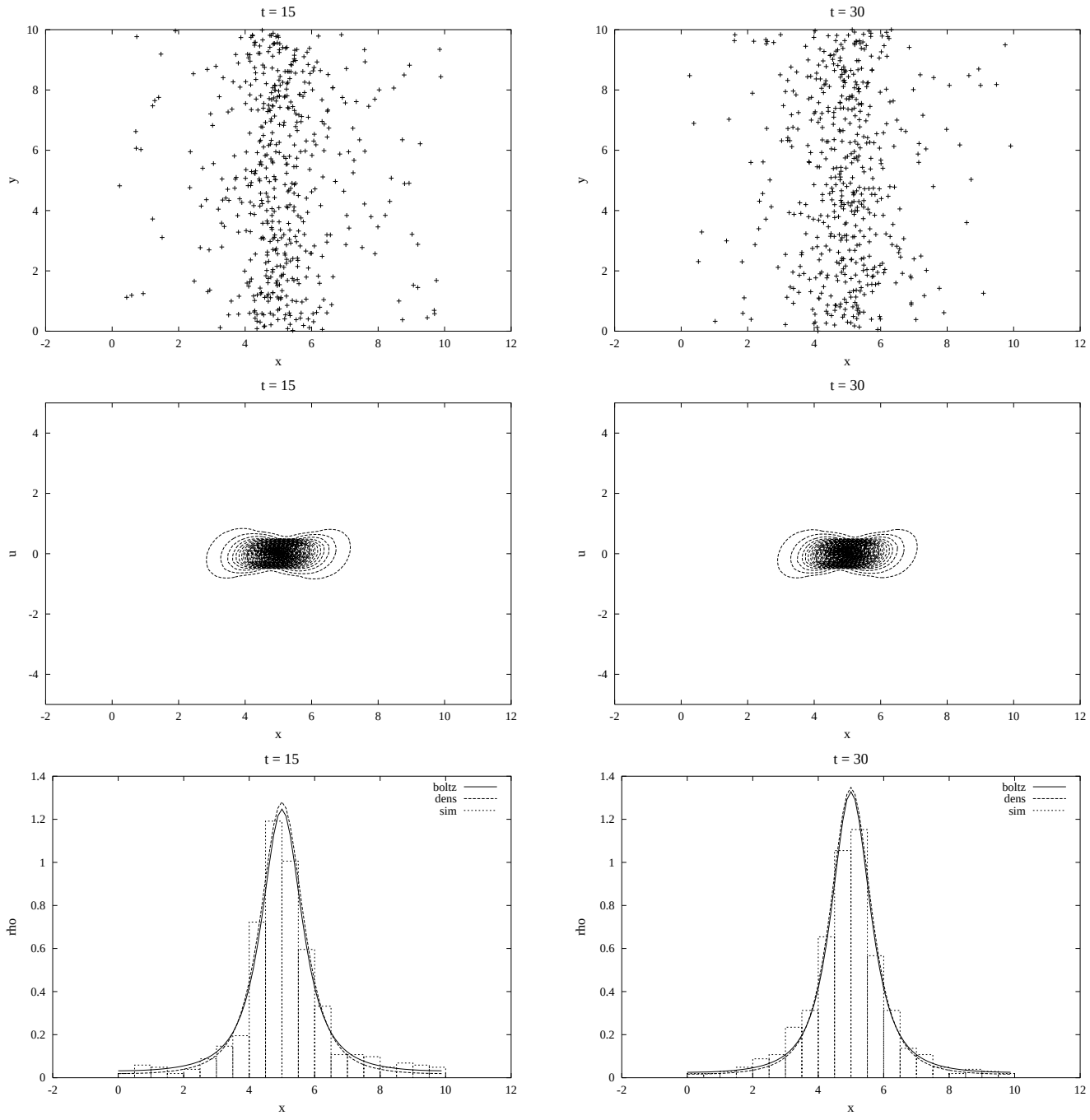

Figure 2.12d: $t = 15,\ 30.$

2.4.2 — Diffusion approximation

Now that we have some sense of the way in which the full probability distribution $\mathcal{P}$ evolves, let us return to the closure issue and derive an approximate equation for the density. We start with the equation for the flux

$$\frac{\partial}{\partial t}J_i = -\frac{\partial}{\partial x_j}\left[N\int d\mathbf{u}\; u_i u_j \mathcal{P}\right] - rJ_i + rV_i b$$

and assume that the relaxation is rapid (large r); then we can use

$$N\mathcal{P} \simeq b(\mathbf{x},t)\mathcal{G}(\mathbf{u}-\mathbf{V}|r\kappa)$$

as a local estimate. This "quasi-normal" approximation allows us to approximate the second moments by

$$N\int d\mathbf{u}\; u_i u_j \mathcal{P} \simeq r\kappa\delta_{ij}b + V_i V_j b \quad .$$

In the appropriate parameter range with r large, the first term dominates so that

$$\frac{\partial}{\partial t}J_i = -\frac{\partial}{\partial x_i}r\kappa b - rJ_i + rV_i b \quad .$$

The flux rapidly relaxes to

$$J_i = V_i b - \frac{1}{r}\frac{\partial}{\partial x_i}(r\kappa b) = \left(V_i - \frac{1}{r}\frac{\partial}{\partial x_i}r\kappa\right)b - \kappa\frac{\partial}{\partial x_i}b$$

with the diffusivity

$$\kappa = \frac{\langle u'^2\rangle}{r}$$

being (c.f. Taylor, 19xx) the product of the variance of the fluctuating velocity and a characteristic time scale $(1/r)$ for the decay of correlations in the fluctuating velocities.

In this limit, we recover the usual biological form of the advection-diffusion equation

$$\frac{\partial}{\partial t}b = -\nabla\cdot[\mathbf{u}_{bio}b - \kappa_{bio}\nabla b] \quad , \quad \mathbf{u}_{bio} = \mathbf{V} - \frac{1}{r}\nabla r\kappa_{bio} \quad , \quad \kappa_{bio} = \frac{\langle \delta U^2\rangle}{2r^2\delta t} = \frac{\langle u'^2\rangle}{r} \quad . \tag{2.16}$$

Going through a formal mathematical treatment (appendix xx) demonstrates that the basic requirement for validity is $rT >> 1$, where T is the characteristic time scale for patch formation or fluid flow changes. The length scale L and the time, velocity and the diffusivity scales satisfy $\mathbf{V} \sim \mathbf{u} \sim L/T$ and $\kappa \sim L^2/T$. One implication is that the r.m.s. velocity fluctuations, which are order $\sqrt{r\kappa} \sim \sqrt{rT}(L/T)$, are large compared to the mean velocities. This assumption – basically equivalent to the mean free path being short compared to the length scales of interest – may not be realistic in some cases; then, diffusion equation results should be viewed with considerable caution.

2.5 — Taxis and Kinesis

To illustrate some of the effects of taxis, we shall study a few simple analytical examples, using the advection-diffusion form. In the absence of flow, these cases will reach a fairly simple balance. Consider organisms with a preferred velocity which is uniformly upwards towards the surface

$$\mathbf{V} = w_0 \hat{\mathbf{z}}$$

and otherwise uniform parameters r and κ. In steady state, the flux J must be uniform and furthermore must be zero since no organisms pass through the surface $z = 0$. Accordingly

$$w_0 b = \kappa \frac{\partial}{\partial z} b \quad \Rightarrow \quad b = b_0 \exp(w_0 z/\kappa)$$

The organisms concentrate near the surface in a layer of characteristic thickness κ/w_0 with the upward swimming balancing downward diffusion.

More generally, suppose the preferred velocity can be written as the gradient of a scalar potential

$$\mathbf{V} = -\nabla \phi \quad ,$$

so that organisms tend to move down into low potential valleys. The steady state (when boundary conditions imply the flux is zero) has local maxima in the low potential regions

$$b = b_0 \exp(-\phi/\kappa)$$

(figure 2.xx). Note that in cases where the cue field is localized so that organisms which are too far away (for example from a patch of food) can no longer determine which direction to swim, the population levels out to a non-zero value. This result implies that a seed population, even in the optimal region, will gradually lose members who wander outside of perception range and then spread further and further out by random walking.

Kinesis also gives rise to particularly simple steady states: if the flux is zero and $\mathbf{V} = 0$, we have

$$\nabla r\kappa b = 0 \quad \Rightarrow \quad b = b_0 \frac{r_0 \kappa_0}{r\kappa} \quad ,$$

so that the density is highest where the velocity variance $r\kappa$ is lowest.

2.5.1 — Diel migration example

Many species of zooplankton have diel migration patterns, living near the surface at night and descending during the day. Suppose the animals swim upwards when the light is less than the optimal level and downwards if it is above

$$\mathbf{V} = w_{bio}\hat{\mathbf{z}} = w_0\hat{\mathbf{z}}\begin{cases} -1 & z > z_0(t) \\ 1 & z < z_0(t) \end{cases} ,$$

where $z_0(t)$ gives the coordinate of the optimal isolume (and is negative during the day). It may be more convenient numerically and more realistic to let the switch from downwards to upwards occur over a finite depth range

$$w_{bio} = -w_0 \tanh\left(\frac{z - z_0(t)}{h}\right) .$$

Analytically, we can consider the case of a steadily rising isolume

$$z_0 = ct$$

(for $t < 0$) and examine the equilibrated density $b = b(z - ct)$. The density equation becomes

$$-c\frac{\partial}{\partial z}b + \frac{\partial}{\partial z}(w_{bio}b) = \frac{\partial}{\partial z}\kappa\frac{\partial}{\partial z}b$$

which can be integrated with respect to z and then treated like the cases above. The solution is

$$b = b_0\begin{cases} \exp\left(\frac{-(w_0+c)(z-ct)}{\kappa}\right) & z > ct \\ \exp\left(\frac{(w_0-c)(z-ct)}{\kappa}\right) & z < ct \end{cases} ,$$

shown in figure 2.xx, along with the solution for the smooth case

$$b = b_0 \exp\left(\frac{-w_0 h \ln \operatorname{sech}\frac{z-ct}{h} + c(z-ct)}{\kappa}\right) .$$

The solutions show a relatively thin layer ahead of the ascending isolume, with a relatively long trail behind it. Above z_0, the velocity relative to the isolume is large, so that a narrow boundary layer is required for diffusion to offset the stronger flow. Below, the relative velocity is smaller and the distribution is wider. When c exceeds w_0, we cannot have a steady solution.

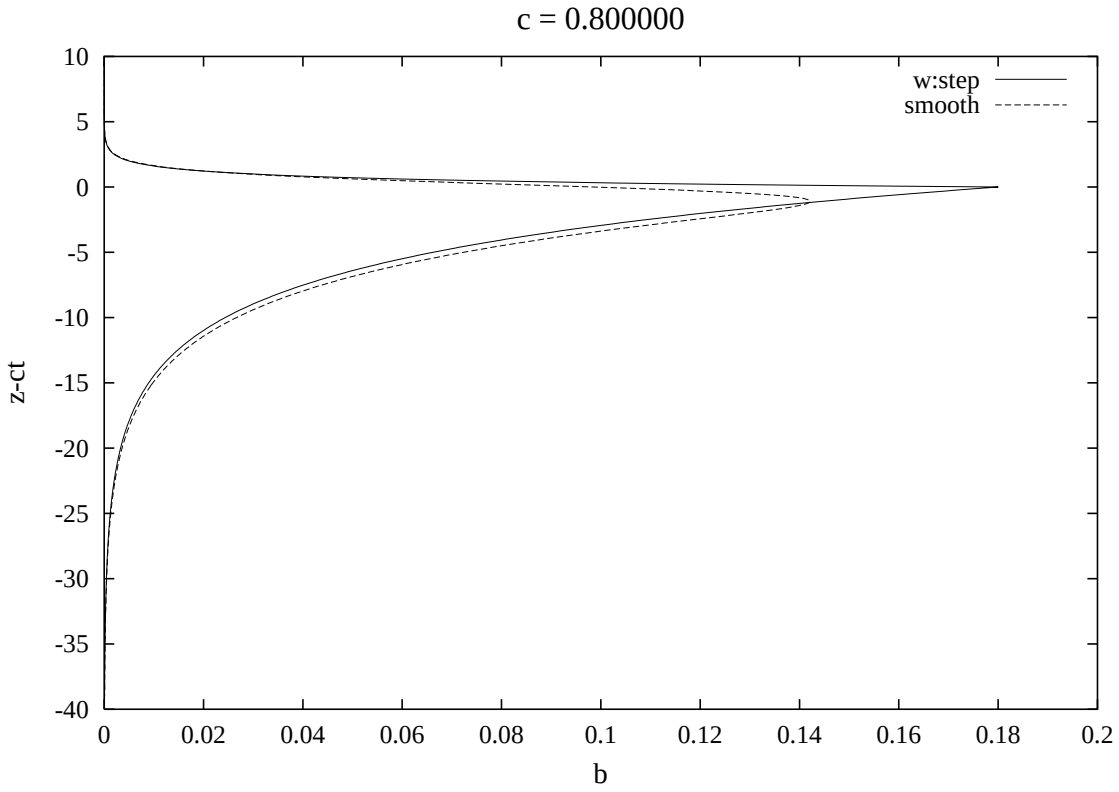

Figure 2.13: Vertical structure when the desired depth is gradually ascending ($c = 0.8 * w_0$).

For a light curve which is zero at night and sinusoidal over the day, we can no longer assume the flux is non-divergent. Assuming that the light decays exponentially with a scale of 17 m and employing a numerical approach results in patterns (figure 2.xx) which cluster about the preferred isolume. Slowly swimming organisms, not surprisingly, have a delayed response so that the minumum surface concentration occurs in the mid-afternoon. The concentrations are highest just before dawn.

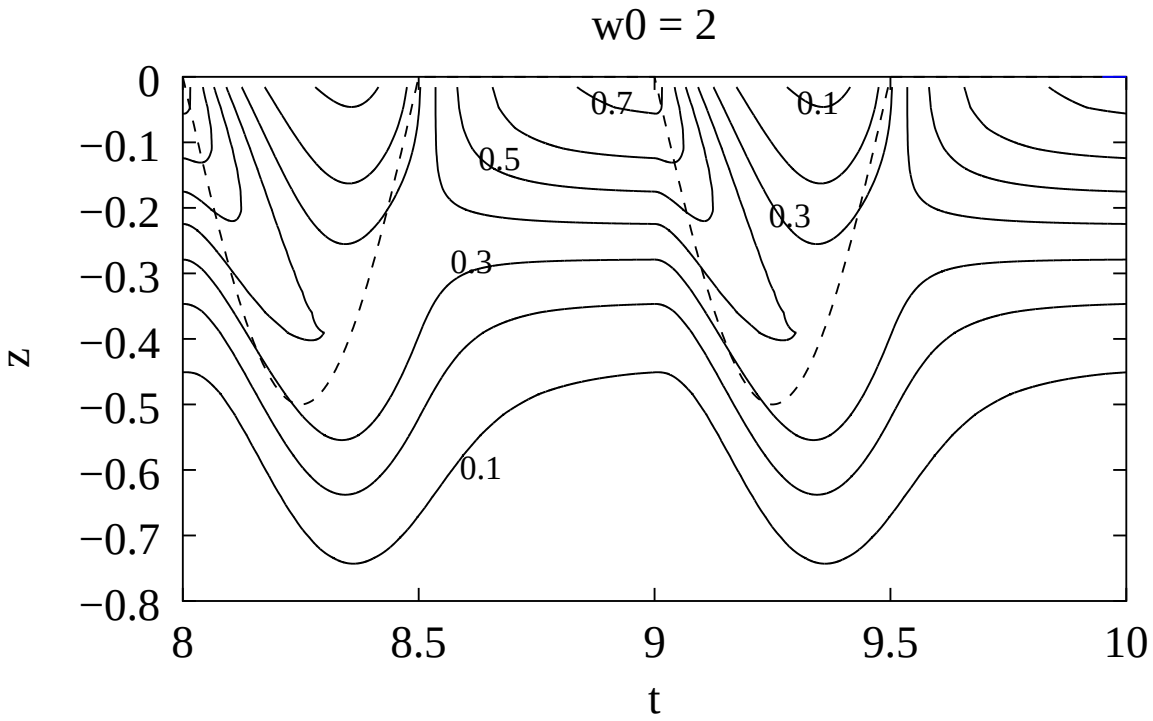

Figure 2.14: Contours of density under diel motion. The dashed line shows the assumed preferred depth (in km), corresponding to a half-sinusoid. $w_0 = 2\ km/d$.

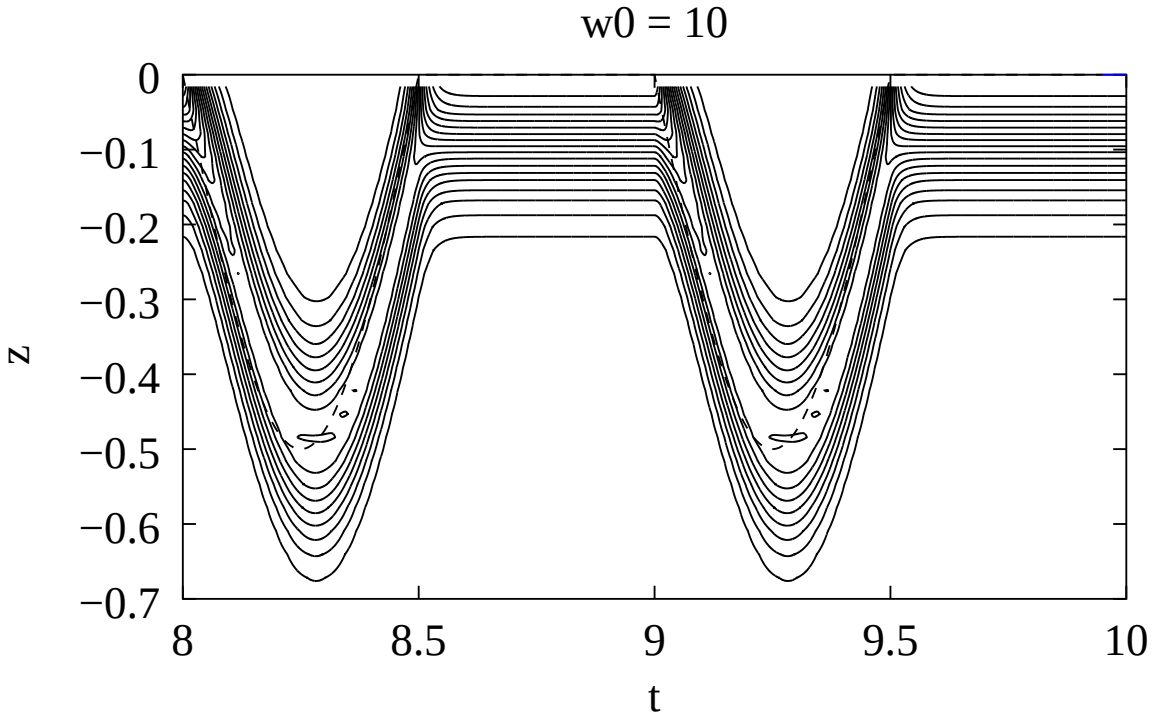

Figure 2.15: Same for $w_0 = 10\ km/d$.

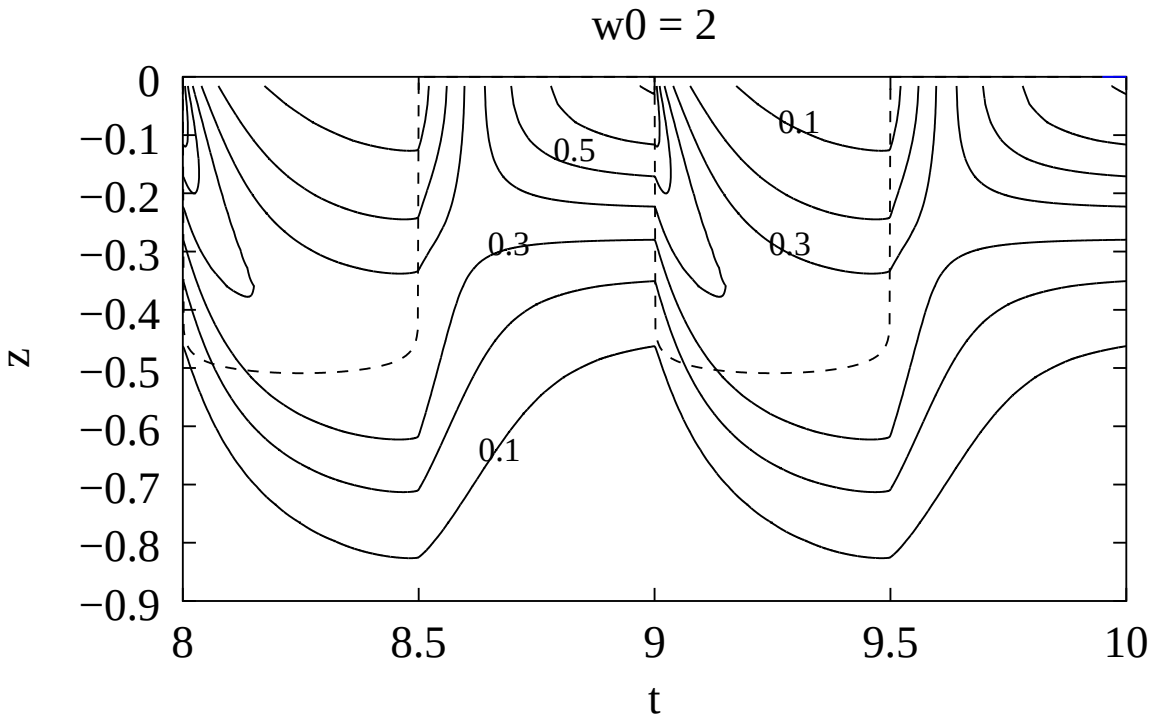

Figure 2.16: Contours of density under diel motion. The dashed line shows the depth of the preferred isolume with 10^{-13} of the surface strength. $w_0 = 2\ km/d$.

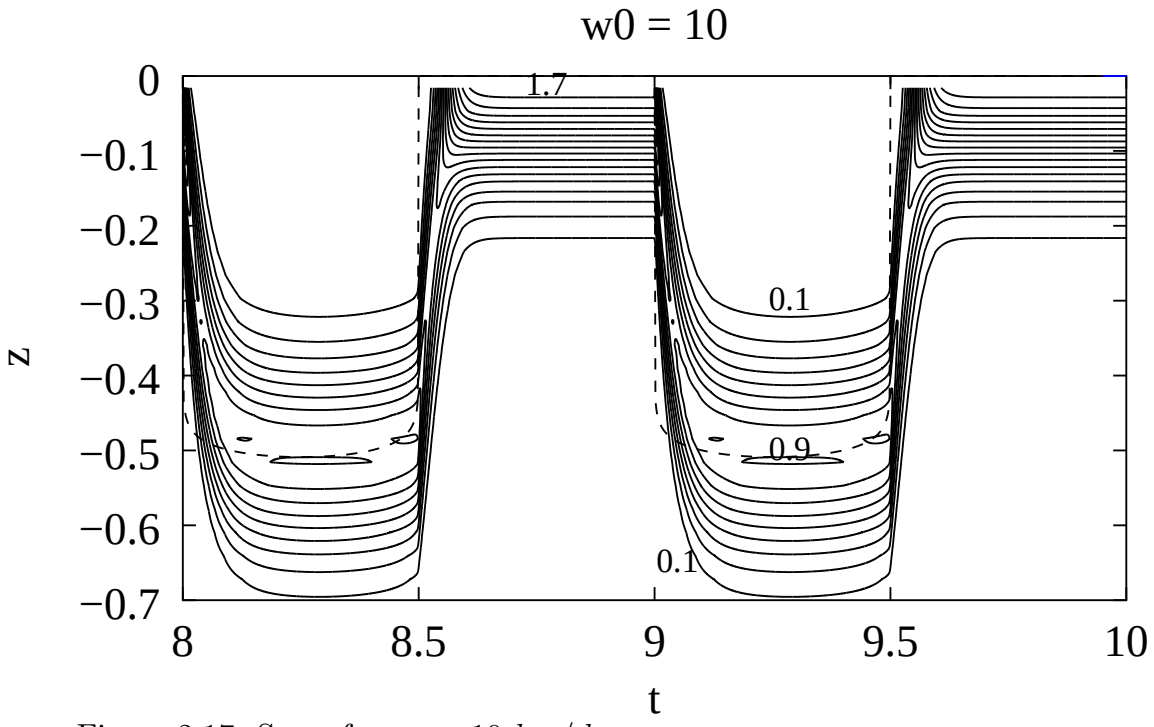

Figure 2.17: Same for $w_0 = 10\ km/d$.

2.5.2 — Social behavior

Biological distributions in the ocean, especially at higher trophic levels, are often patchy, so that the distribution of organisms is distinctly not random: individuals have more close neighbors than one would expect and large areas have lower than average density. Figure 2.xx illustrates a random versus a patchy distribution with the same density. Also shown are several measures which quantitatively demonstrate the difference in character.

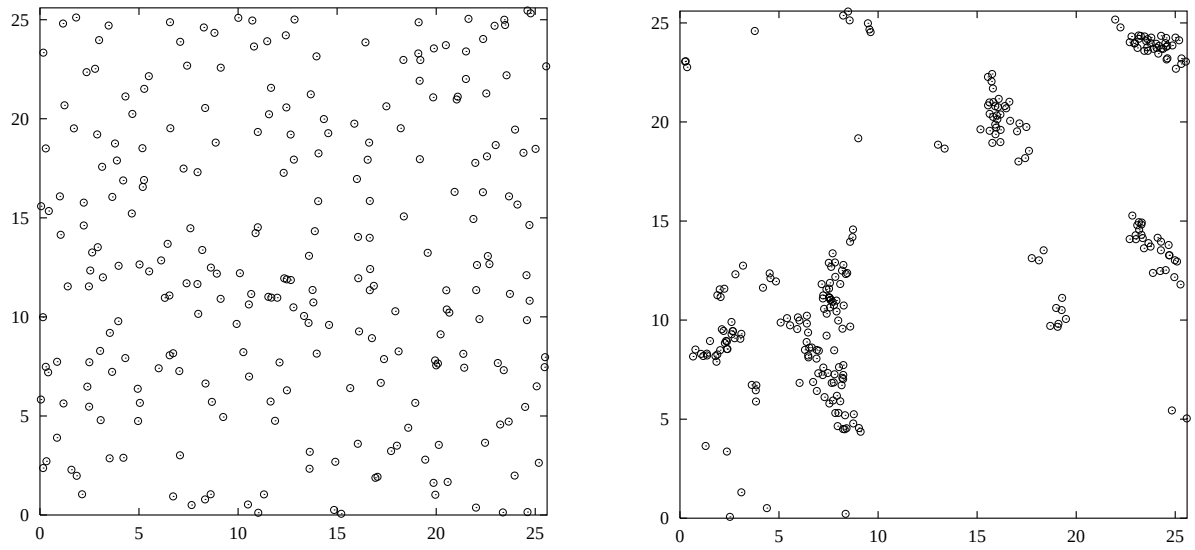

Figure 2.18a: Random and patchy distributions

Patchiness can arise from both biological and physical mechanisms. Stirring can lead to streaky patterns (e.g. figure xx.xx); for example, organisms spawned near the coast can be pulled offshore in narrow plumes and end up as high density parches in otherwise clear water. Biologically, organisms whose offspring are born near the parent (e.g. phytoplankton which reproduce by fission), form clusters from "demographic stochasticity" (Young, 2000) – local extinctions occur, causing empty areas, while patches become more dense as reproduction occurs. Behavior, here meaning movement patterns which vary as the environment changes, can also cause aggregations. When the cue causing alteration in movement is associated with the presence and perhaps characteristics of neighbors of the same species, self-organizing structures can arise. This "social behavior" is common among larger zooplankton and fish; we shall explore the resulting dynamics, but caution that the ecological and evolutionary significance of these processes are not fully understood.

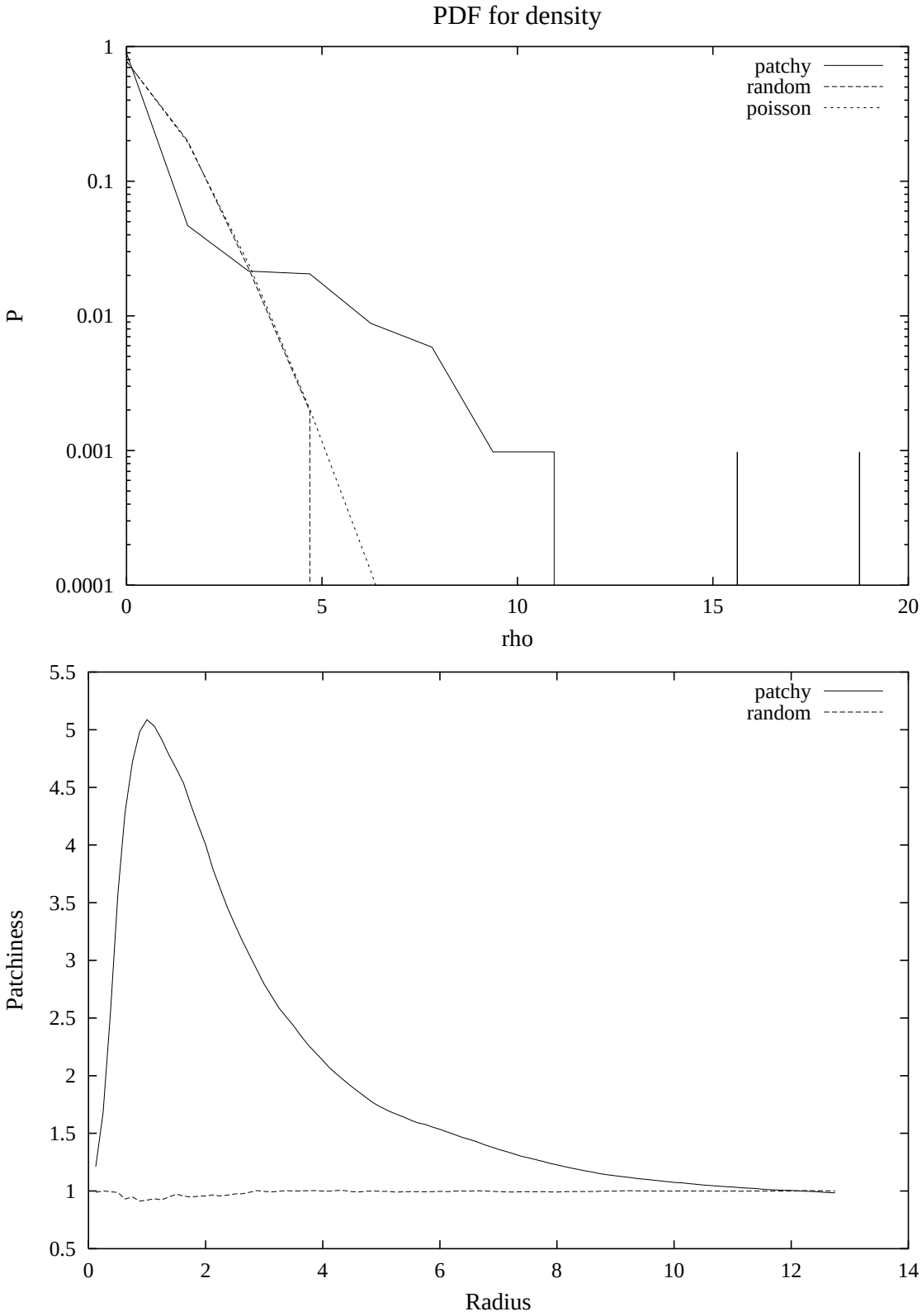

Figure 2.18b: Patchiness indices: probability for density in squares of scale $L/32$ and Lloyd's patchiness index (number of neighbors in a circle of radius R divided by the expected number for a Poisson process).

Social kinesis

The simplest case we can analyze is social kinesis, in which the cue (denoted by ϕ) causing the organisms to alter their behavior is related to the density of neighbors within the perception distance. For discrete individuals, we can take

$$\phi(\mathbf{X}_i) = f(R) \quad , \qquad R = \sum_{j \neq i} \mathcal{W}(|\mathbf{X}_j - \mathbf{X}_i|) \quad . \tag{2.17}$$

The weighting function is zero for distances greater than the perception distance. Kinesis involves a decrease in the random hop $\delta\mathbf{X}_i$ or random acceleration $\delta\mathbf{U}_i$ of the i^{th} organism as the desirability of a particular spot – represented by $\phi(\mathbf{X}_i)$ – increases.

We shall use the random flight model 2.xx with $\langle \delta U_i \delta U_j \rangle = 2\delta_{ij}\mathcal{K}\delta t$ and

$$\mathcal{K} = \mathcal{K}_0 \exp(-\beta\phi) \quad .$$

The deterministic term is again $-rU_i$, causing the movements to damp out in the absence of stochastic accelerations. Since we have very little information on how these organisms perceive, we are forced to fall back to simply postulation various functions for $\mathcal{W}$ and f and seeing in what ways they are similar or different. Consider four cases:

1) a simple weighting function $\mathcal{W}(d) = \frac{2}{\pi}(1 - d^2)$ with the cue just a linear function $\phi = R$. Distances are measured in terms of perception lengths.
2) a weighting function $\mathcal{W}(d) = \frac{9}{\pi}(1 - d^2)(d^2 - \frac{1}{9})$ representing "personal space" so that neighbors which are too close will cause the accelerations to increase again.
3) a saturation of the cue as the number of neighbors increases

$$\phi = \phi_{max} \frac{R}{\phi_{max} + R}$$

   This form incorporates appropriate limitations on the perceptive abilities: zooplankton can probably distinguish between a few neighbors and many neighbors, but their response saturates so that their behavior is similar whether they have (say) 10, 20, or 100 neighbors — $\mathcal{K} = \mathcal{K}_0 \exp(-\beta\phi_{max})$.
4) a cue which initially increases with density, but decreases again as the density becomes too high, so that the region is no longer desirable.

$$\phi = Re^{-R/e\phi_{max}}$$

Figure 2.xx shows an example from each case with $\beta = 5$, $\phi_{max} = 1$, $\rho = 1$, and $\mathcal{K}_0 = 1$. Note that case 1 yields very small, densly packed groups, while the examples from cases 3 and 4, where the reponse saturates, have much looser clusters (although they become tighter as ϕ_{max} increases). The groups also move more and split or merge.

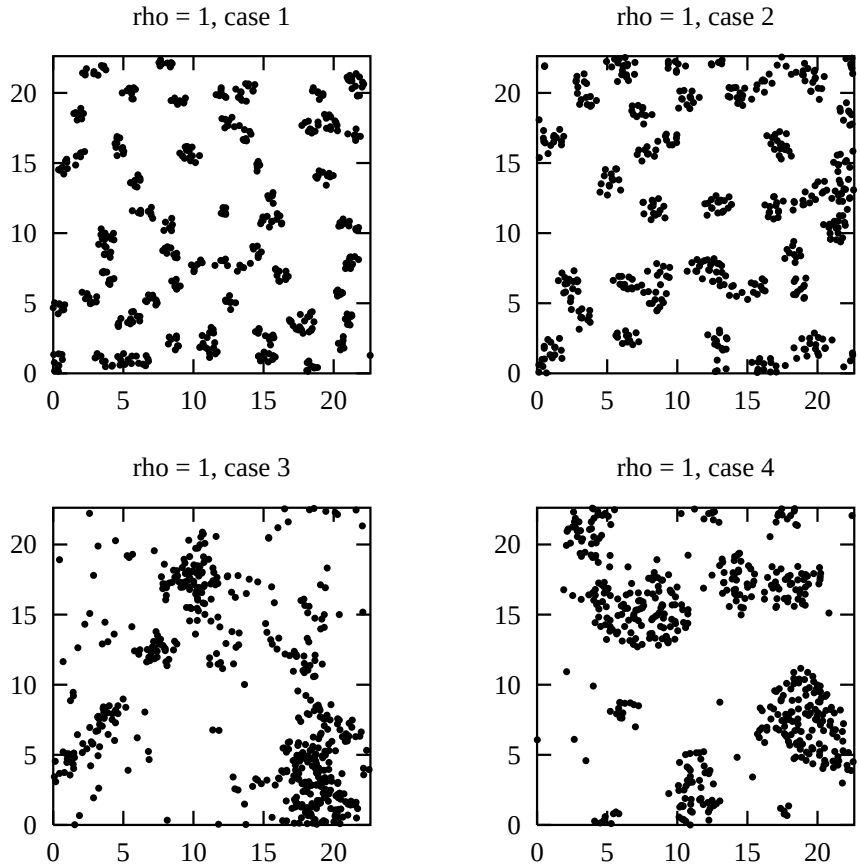

Figure 2.19: Simulations for different types of kinesis response. The domain is doubly periodic.

Figure 2.xx shows the result from direct simulations of the 2D random flight model 2.xx with $\langle \delta U_i \delta U_j \rangle = 2\delta_{ij}\mathcal{K}\delta t$ for various population densities using the third case above. As the density increases, the pattern switches from essentially random distributions to spontaneous formation of patches. The critical density will depend on the parameters $\mathcal{K}_0,\ \beta,\ r$ as well as the details of the weighting function, $\mathcal{W}$ and the form of $\phi(R)$.

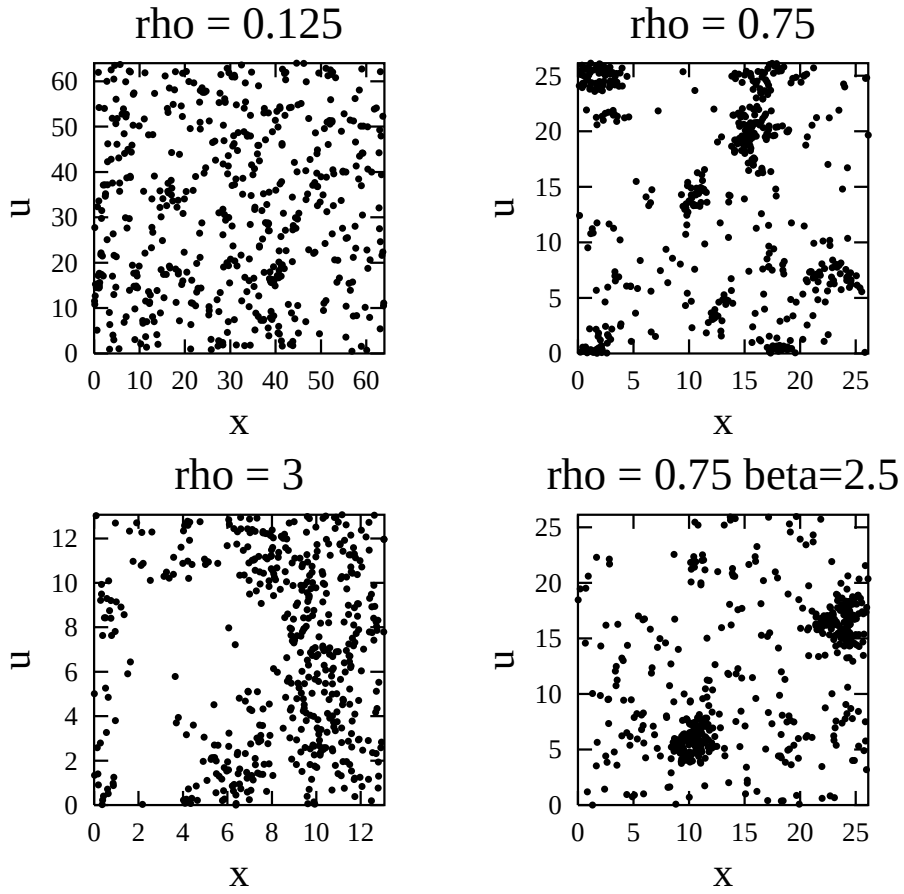

Figure 2.20: Simulations at different densities (note different scales) with $r = 1$ and $\kappa_0 = 1$. Except for the lower right figure, $\beta = 5$ and $\phi_{max} = 1$; in the last case, $\beta = 2.5$ and $\phi_{max} = 2$, indicating that the important parameter is the product of the two.

To find the critical density and relate it to the parameters, let us consider the continuum version of the problem. The approximations discussed above lead to a density equation

$$\frac{\partial}{\partial t}\rho = -\nabla \cdot \mathbf{J} \quad , \quad \mathbf{J} = -\frac{1}{r}\nabla\left(\frac{\mathcal{K}}{r}\rho\right) \quad .$$

The estimated density of neighbors withing the perception distance is found by replacing the weighted sum 2.xx with a convolution integral

$$R(\mathbf{x}) = \int d\mathbf{z}\, \mathcal{W}(\mathbf{z})\rho(\mathbf{x}+\mathbf{z}) \quad .$$

STABILITY:

Under what conditions will the uniform state $\rho(\mathbf{x}) = \overline{\rho}$ break up into patches? This is again a stability problem, but now with the addition of spatial variability. First, we need to demonstrate that a state with uniform density is a steady solution. For $\rho = \overline{\rho}$, the estimated local density is

$$R = \int d\mathbf{z}\, \mathcal{W}(\mathbf{z})\overline{\rho} = \overline{\rho} \quad ,$$

so that ϕ and $\mathcal{K}$ are also constants. The flux $\mathbf{J}$ is then zero, and $\frac{\partial}{\partial t}\rho$ is indeed zero.

Now we perturb the steady state

$$\rho = \overline{\rho} + \rho'(\mathbf{x}, t)$$

and calculate the terms which appear in the density equation

$$\frac{\partial}{\partial t}\rho' = \frac{1}{r^2}\nabla^2(\overline{\mathcal{K}}\rho' + \mathcal{K}'\overline{\rho}) \quad .$$

The first term will damp out perturbations; growth can only occur when $\mathcal{K}'$ and ρ' are negatively correlated. To calculate this correlation, we can use separation of variables

$$\rho' = \rho_0 \exp(\imath\mathbf{k}\cdot\mathbf{x}) \exp(\sigma t) \quad .$$

The exponential form arises naturally because the equations are homogeneous in both space and time – the stochastic term $\mathcal{K}$ does not explicitly depend on $\mathbf{x}$ or t, and the weighting function only varies with separation. (We can certainly think of counterexamples – e.g., when the movements combine social behavior with sensitivity to external conditions such as food concentration.) From this form for the perturbations, the estimated local density becomes

$$R = \overline{\rho} + \hat{\mathcal{W}}(|\mathbf{k}|)\rho' \quad , \quad \hat{\mathcal{W}}(|\mathbf{k}|) = \int d\mathbf{z}\, \mathcal{W}(\mathbf{z}) \exp(\imath\mathbf{k}\cdot\mathbf{z}) \quad ,$$

so that

$$\mathcal{K}' = \frac{\partial\mathcal{K}}{\partial\phi}\frac{\partial\phi}{\partial R}\hat{\mathcal{W}}(|\mathbf{k}|)\rho' = -\beta\overline{\mathcal{K}}\frac{\partial\phi}{\partial R}\hat{\mathcal{W}}(|\mathbf{k}|)\rho' \quad .$$

From these, we find

$$\sigma = -\frac{1}{r^2}|\mathbf{k}|^2 \left[\overline{\mathcal{K}} - \overline{\rho}\beta\overline{\mathcal{K}}\frac{\partial\phi}{\partial R}\hat{\mathcal{W}}(|\mathbf{k}|)\right] \quad ,$$

which demonstrates that small perturbations will grow exponentially when

$$\overline{\rho}\beta\frac{\partial\phi}{\partial R}\hat{\mathcal{W}}(|\mathbf{k}|) > 1 \quad .$$

Figure 2.xx shows that when the density exceeds the critical value $\left(\beta\frac{\partial\phi}{\partial R}\right)^{-1}$, the long waves become unstable. For slightly larger values of $\overline{\rho}$, however, the patches with a scale on the order of the perception distance are favored. For example, in the case 3 where the

desirability of a spot levels off as the local density increases, the maximum growth (for $\beta\phi_{max} = 5$) occurs when $\overline{\rho} \sim \phi_{max}$ and $k = 1.12$, corresponding to a spacing between patches of 5.6 times the perception distance. For this model, grouping does not occur when the density is very large, since the diffusivity becomes very small $\sim \mathcal{K}_0 \exp(-\beta\phi_{max})$ everywhere, and the variations are too weak to have much effect. The simulations show a slow decay in patchiness as the density increases (figure 2.xx).

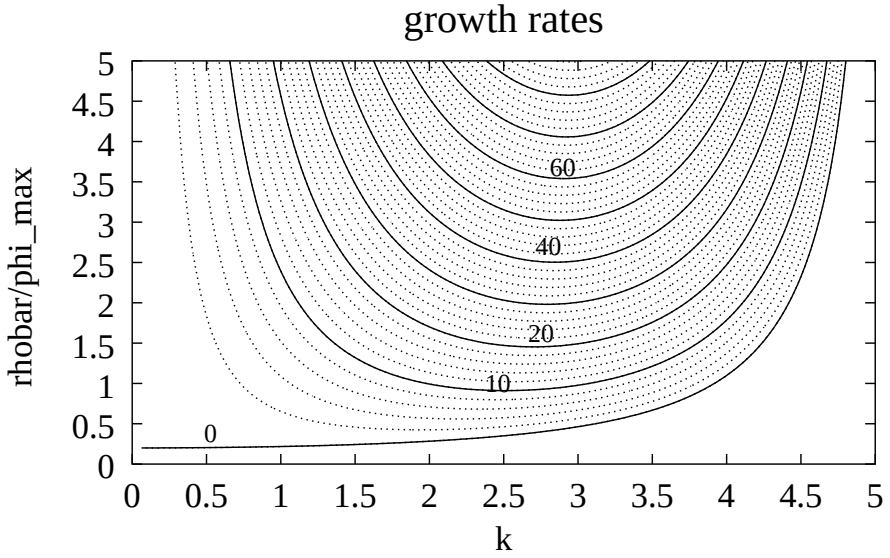

Figure 2.21a: Case 1 growth rates as a function of k (normalized by the perception distance) and $\overline{\rho}/\phi_{max}$. Here $\beta\phi_{max} = 5$.

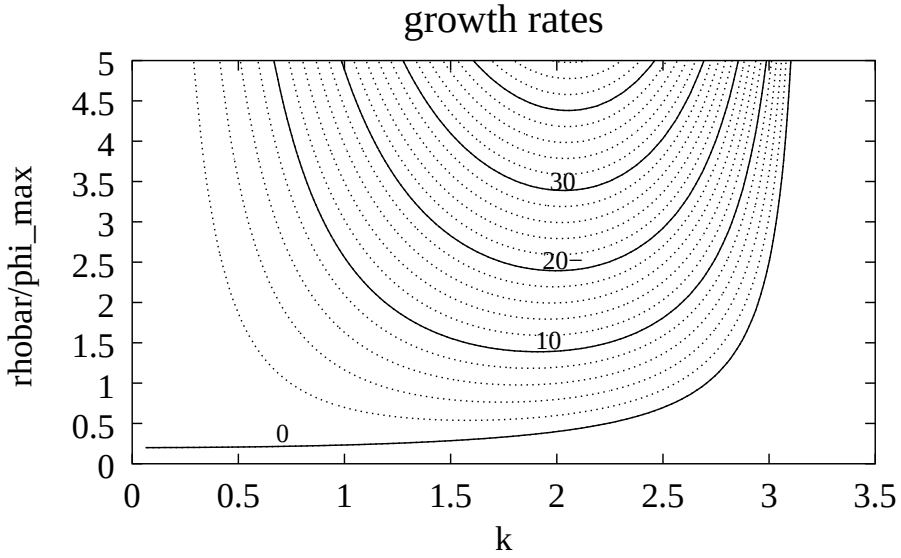

Figure 2.21b: Case 2 growth rates.

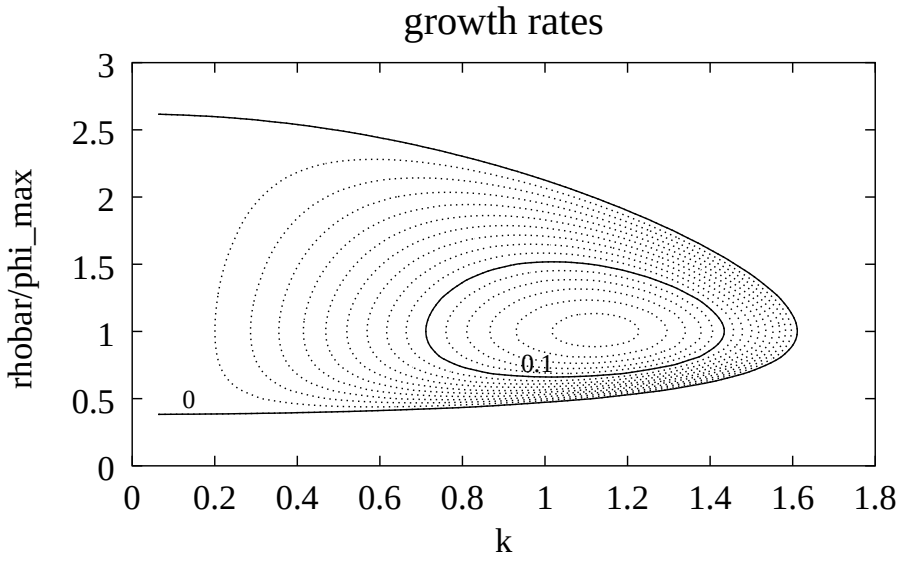

Figure 2.21c: Case 3 growth rates.

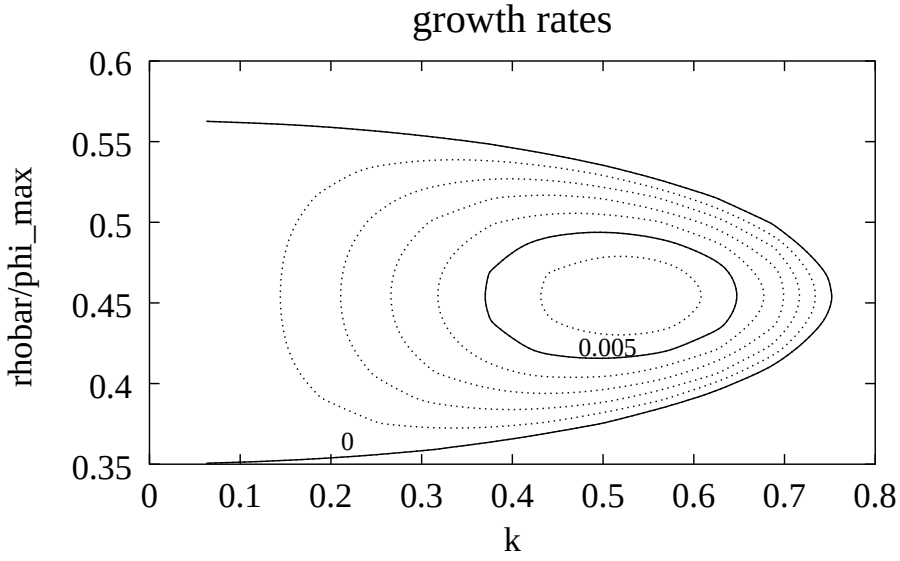

Figure 2.21d: Case 4 growth rates.

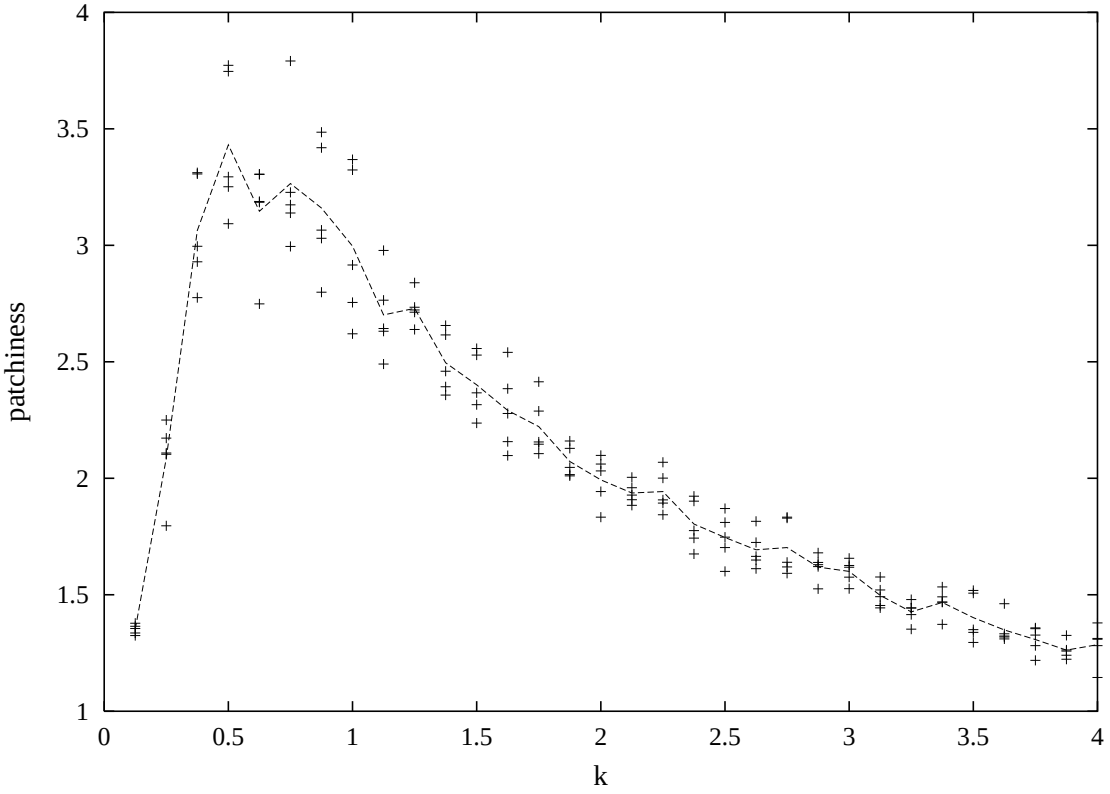

Figure 2.22: Individual-based simulations of case 3 with $\beta\phi_{max} = 5$ for different densities. The points show the patchiness averaged over $t = 800$—1000 for five realizations at each density; the line gives the average.

Social taxis

When the organisms modify their swimming based on gradients in the neighbor densities (i.e., they aim in the direction where they see more congeners), they can form also form dense aggregations. To model this kind of social taxis, we take the preferred velocity to have the form

$$\mathbf{V}_i = \mathbf{f}(\mathbf{R}_i) \quad , \quad \mathbf{R}_i = \sum_{j \neq i} (\mathbf{X}_j - \mathbf{X}_i) \mathcal{W}(|\mathbf{X}_j - \mathbf{X}_i|) \quad .$$

As in the previous case of kinesis, we face the same issues of deciding on a reasonable form for the weighting function and on limitations in perceptive abilities and swimming speeds. We can write $\mathbf{R}$ as the gradient with respect to $\mathbf{X}_i$ of a scalar function

$$\mathbf{R} = \frac{\partial}{\partial X_i} \sum W(|\mathbf{X}_j - \mathbf{X}_i|) = \frac{\partial \phi}{\partial X_i} \quad , \quad W'(s) = -s\mathcal{W}(s) \quad .$$

Then, in the simplest case where $\mathbf{V}$ is a linear function of $\mathbf{R}$, the continuum equations become

$$\frac{\partial}{\partial t}\rho = -\nabla \cdot [\rho \nabla \phi - \kappa \nabla \rho]$$

which can be analyzed in exactly the same way as the case of kinesis. We can impose perceptive limitations (e.g., by making ϕ saturate for large values of $\int d\mathbf{x}' W(\mathbf{x}-\mathbf{x}')\rho(\mathbf{x}'))$ or restrictions on swimming ability (letting f be a nonlinear function of $\nabla\phi$); however, the behaviors are qualitatively similar to those produced by kinesis.

Schooling

Schooling is a more sophisticated form of social behavior in which organisms not only aggregate in patches but tend to be aligned in similar directions and to move with similar velocities. In the simplest form, we can take the preferred velocity to be a weighted sum of the neighbors' velocity vectors; moreover, the resulting schools are rather amorphous and short-lived. Adding an additional taxis based on neighbor positions

$$\hat{\mathbf{V}}_i = \sum_{i\neq j} \mathbf{U}_j \mathcal{W}(|\mathbf{X}_i - \mathbf{X}_j|) + \delta \sum_{i\neq j} (\mathbf{X}_j - X_i)\mathcal{W}(|\mathbf{X}_i - \mathbf{X}_j|)$$

and normalizing

$$\mathbf{V}_i = V_0 \frac{\hat{\mathbf{V}}_i}{\sqrt{|\hat{\mathbf{V}}_i|^2 + 0.001}}$$

generates more realistic schools (figure 2.xx). (For reference, an organism swims a single sensing distance in 5 time units.) Schools can merge or break apart; individuals can join or leave. Figure 2.xx illustrates the changes in cluster size which occur by these processes in a set of realizations with $\delta = 0.3$, $\kappa = 0.014$, and $V_0 = 0.2$. After the initial phase, the statistics of the schools settle, with 20-30 clusters in the domain; on average, these clusters have on the order of 35 members, with the largest running on the order of 200-300 individuals.

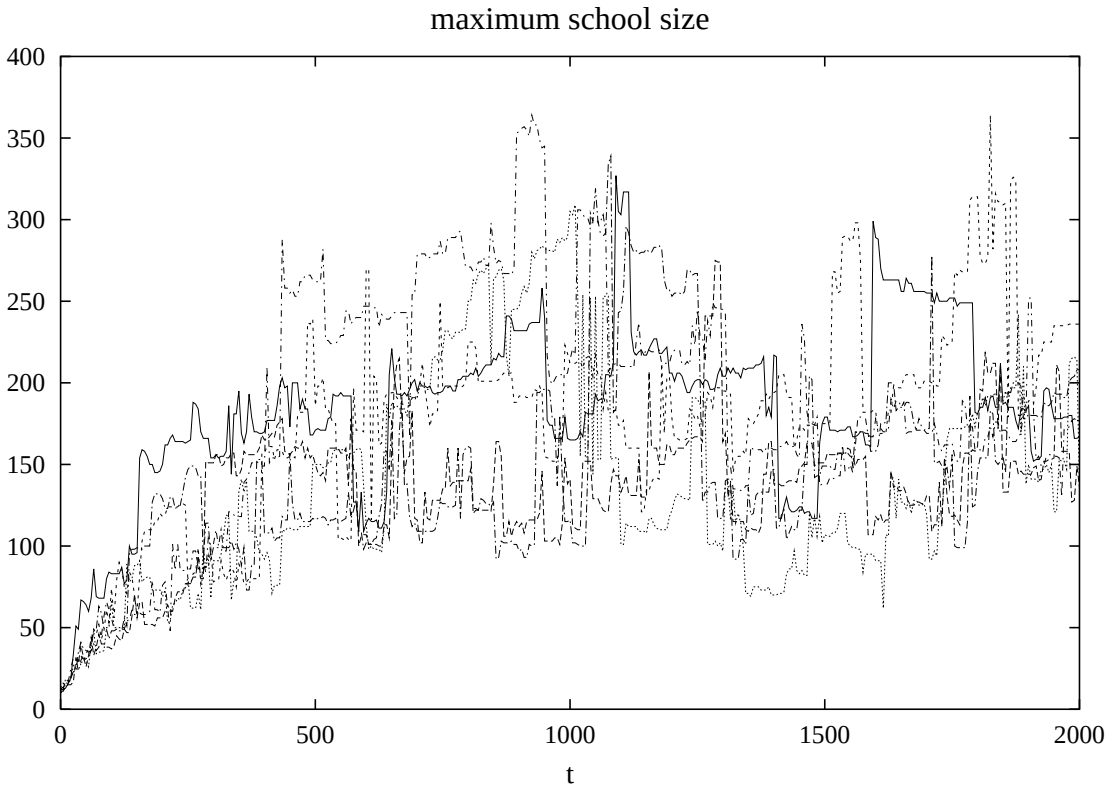

Figure 2.23: Schooling experiments with 1024 individuals in a domain 51.2 times the sensing radius. Note the jumps in size as the largest school merges with another or splits apart.

As xxx (19xx) have pointed out, these kinds of experiments can be used to derive empirically a dynamics for groups, meaning the propagation, splitting and merger rates, all of which depend on the sizes of the schools and the number of schools per unit area. Merger can be predicted from estimated encounter rates. To illustrate splitting, we have run a series of experiments starting with a (highly artificial) school of N organisms within a square with sides equal to one sensing radius and with identical velocities. After a short time, the schools adopt the more elongated pattern seen in figure 2.xx. The velocities of the schools decreases very slightly as we vary the number from 64 to 128 to 256. But the time before a second school breaks off averages 123, 168, and 169 for the different (increasing) school sizes. (One of the smallest schools lasted for more than 700 time units.)

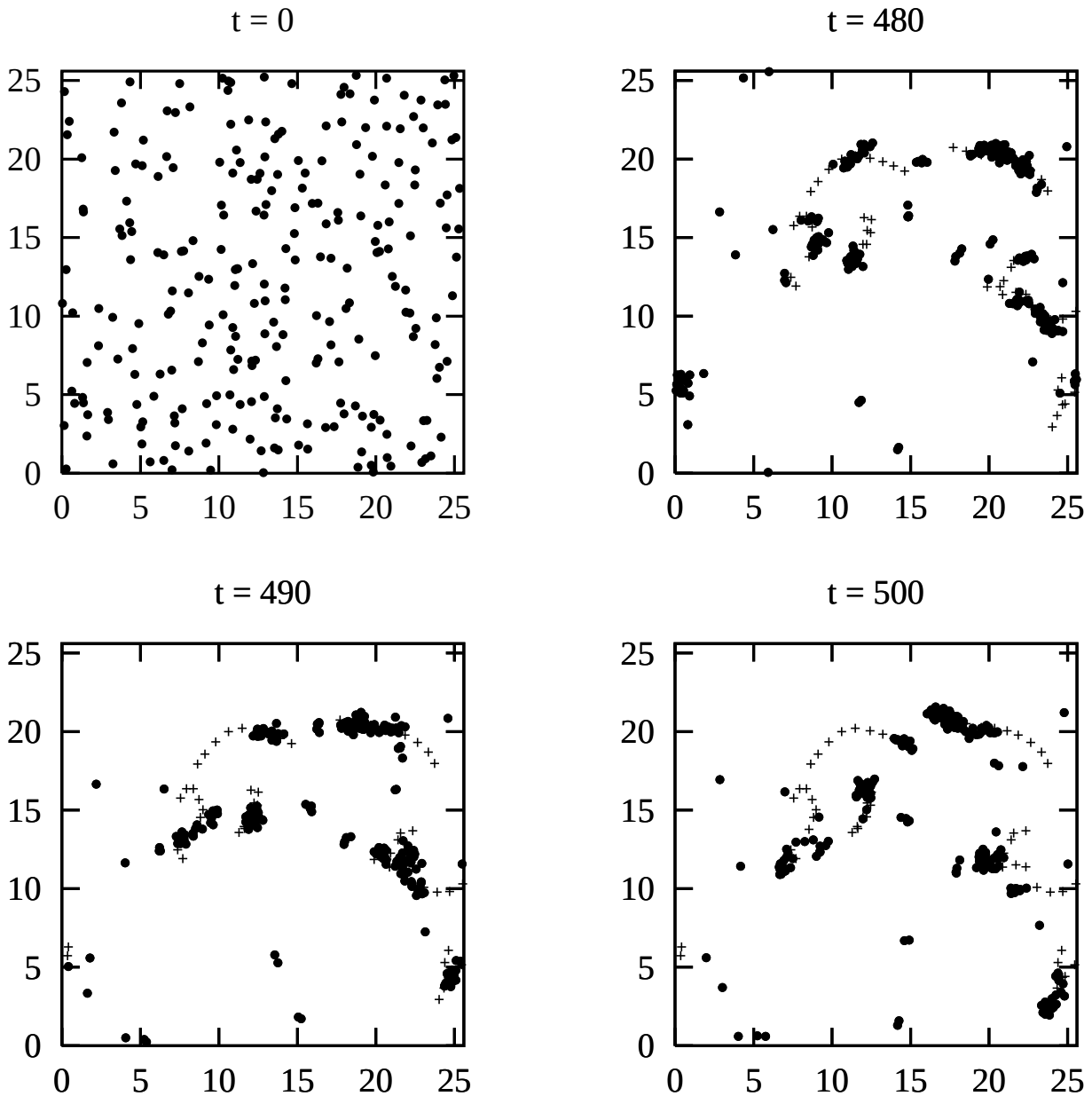

Figure 2.24: Schooling with $V_0 = 0.2$, $\mathcal{W}(r) = \frac{2}{\pi}(1-r^2)$, $\delta = 0.4$, $r = 1$, $\kappa = 0.014$. The + signs show the trajectory for $t \geq 460$ of the centers of the schools, defined as sets of at least 10 individuals who are no more than one sensing distance form at least one other member of the school.

2.6 — Some effects of movement on biological interactions

We began the chapter by discussing the importance of movement on biological distributions; now that we have examined various types of movement, let us explore some of the consequences.

Vertical migration

As an example of the effects of vertical swimming, let us consider the Quadratic NPZ model with the zooplankton having a constant upward or downward velocity w_0

$$\begin{aligned}
\frac{\partial}{\partial t}P &= P\big[\mu N - gZ - d_p\big] + \frac{\partial}{\partial z}\kappa\frac{\partial}{\partial z}P \\
\frac{\partial}{\partial t}Z + \frac{\partial}{\partial z}(w_0 Z) &= Z\big[agP - d_Z\big] + \frac{\partial}{\partial z}\kappa\frac{\partial}{\partial z}Z \\
\frac{\partial}{\partial t}N &= -\mu PN + (1-a)gPZ + d_P P + d_Z Z + \frac{\partial}{\partial z}\kappa\frac{\partial}{\partial z}N \quad .
\end{aligned}$$

When the zooplankton swim upwards, they equilibrate at higher biomass levels, and the total amount of nutrient, $P + Z + N$, is no longer uniform, but becomes higher in the euphotic zone and lower in the deep water (figure 2.xx). Upward swimming results in a 57% increase in the net zooplankton biomass by allowing them to resist the diffusion into the deep, food-poor regions; downward swimming reduces the net Z biomass by 34%.

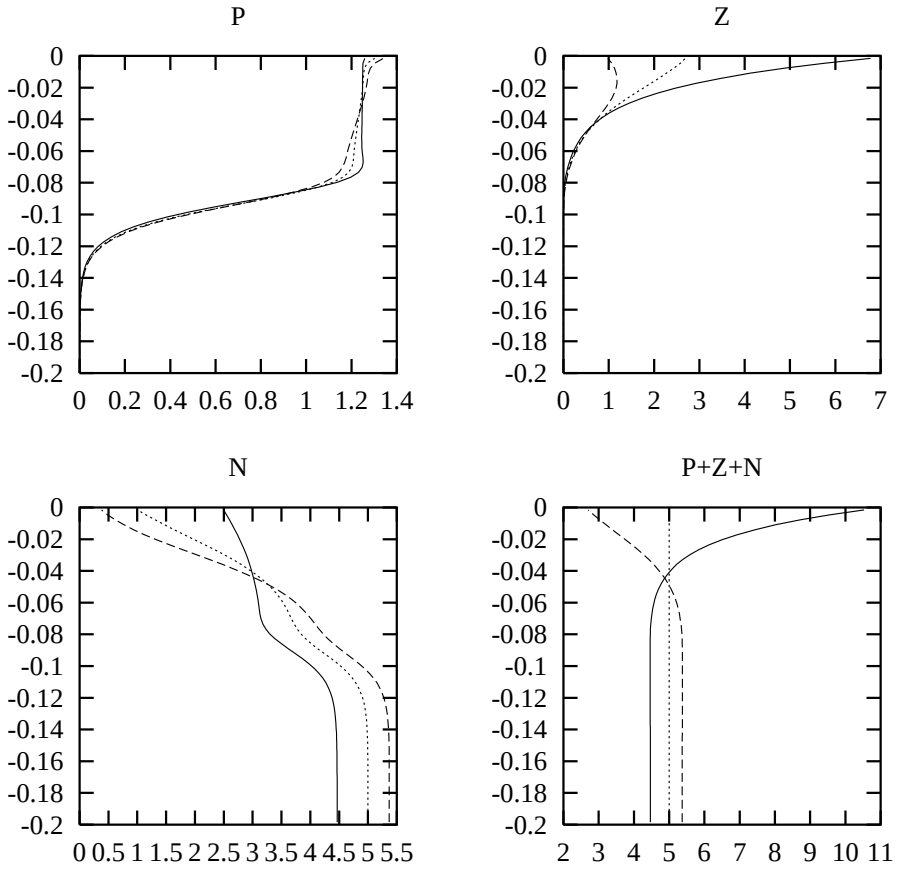

Figure 2.25: Effects of vertical swimming in the QNPZ model. The solid/ dotted/ dashed lines show the cases $w_0 = 5 \times 10^{-5}\ km/d$, 0, and $-5 \times 10^{-5}\ km/d$, respectively.

Schooling and feeding

As a second example, we will examine how schooling behavior alters the grazing rate for zooplankton. We shall use a mixed model, in which the zooplankton are represented as individuals and the phytoplankton as a field. However, the continuum model can give some insight. Suppose the phytoplankton equation has logistic growth and grazing[†]

$$\frac{\partial}{\partial t}P = \mu P\left(1 - \frac{P}{P_0}\right) - gPZ \tag{2.18}$$

and split P and Z into the average values (area or ensemble) and the deviations. Taking the averages of the $\frac{\partial}{\partial t}P$ and the $\frac{1}{P}\frac{\partial}{\partial t}P$ equations results in

$$\begin{aligned}\frac{\partial}{\partial t}\langle P\rangle &= \mu\langle P\rangle - \mu\frac{\langle P\rangle^2}{P_0} - \mu\frac{\langle P'^2\rangle}{P_0} - g\langle P\rangle\langle Z\rangle - g\langle P'Z'\rangle \\ \frac{\partial}{\partial t}\langle \ln P\rangle &= \mu - \mu\frac{\langle P\rangle}{P_0} - g\langle Z\rangle \quad .\end{aligned}$$

If the system reaches a statistically steady state, the $\frac{\partial}{\partial t}$ terms vanish, and the average phytoplankton and zooplankton values bear the same relationship to each other as in the spatially uniform case:

$$\langle P\rangle = P_0\left(1 - \frac{g\langle Z\rangle}{\mu}\right) \quad .$$

Multiplying the second equation by $\langle P\rangle$ and subtracting from the first demonstrates that the spatial variability – the deviations from the mean – contributes negatively to the grazing rate

$$g\langle P'Z'\rangle = -\mu\frac{\langle P'^2\rangle}{P_0} < 0 \quad .$$

The average grazing rate will be lower than that of uniformly distributed zooplankton with density $\langle Z\rangle$, even though the average phytoplankton concentration remains the same.

To see how much the rate decreases, we combine the schooling model with the plankton equation (2.xx). We partition the domain into small squares and count the number of zooplankton in each square; dividing by the size of the square provides the local concentration Z. We solve equation (2.xx) by rewriting it in terms of $S = 1/P$

$$\frac{\partial}{\partial t}S = -(\mu - gZ)S + \mu \quad ,$$

[†] The quadratic NPZ model xx.xx can be written in this form by suitably redefining the constants.

which can be solved exactly over time δt (assuming negligible changes in Z)

$$S(t+\delta t) = \frac{\mu}{\mu - gZ} + \left(S(t) - \frac{\mu}{\mu - gZ} \right) \exp(-[\mu - gZ]\delta t) \quad .$$

Figure (2.xx) shows the schools leaving a trail of depleted food supply, P, as they move though the domain; the length of these depend on the rate of movement ($\sim V_0$), the density in the patches (order 10 times the mean for this experiment), the grazing rate, and the phytoplankton recovery time. For this experiment, the average grazing rate is reduced by 73%. Even the "null experiment" in which the zooplankton swim randomly ($\mathbf{V}_i$ is chosen to be $V_0(\cos\theta_i,\ \sin\theta_i)$ with θ_i chosen randomly from 0 to 2π at each time step) has a reduced grazing rate on the average – about 20% less than that predicted by the products of the means.

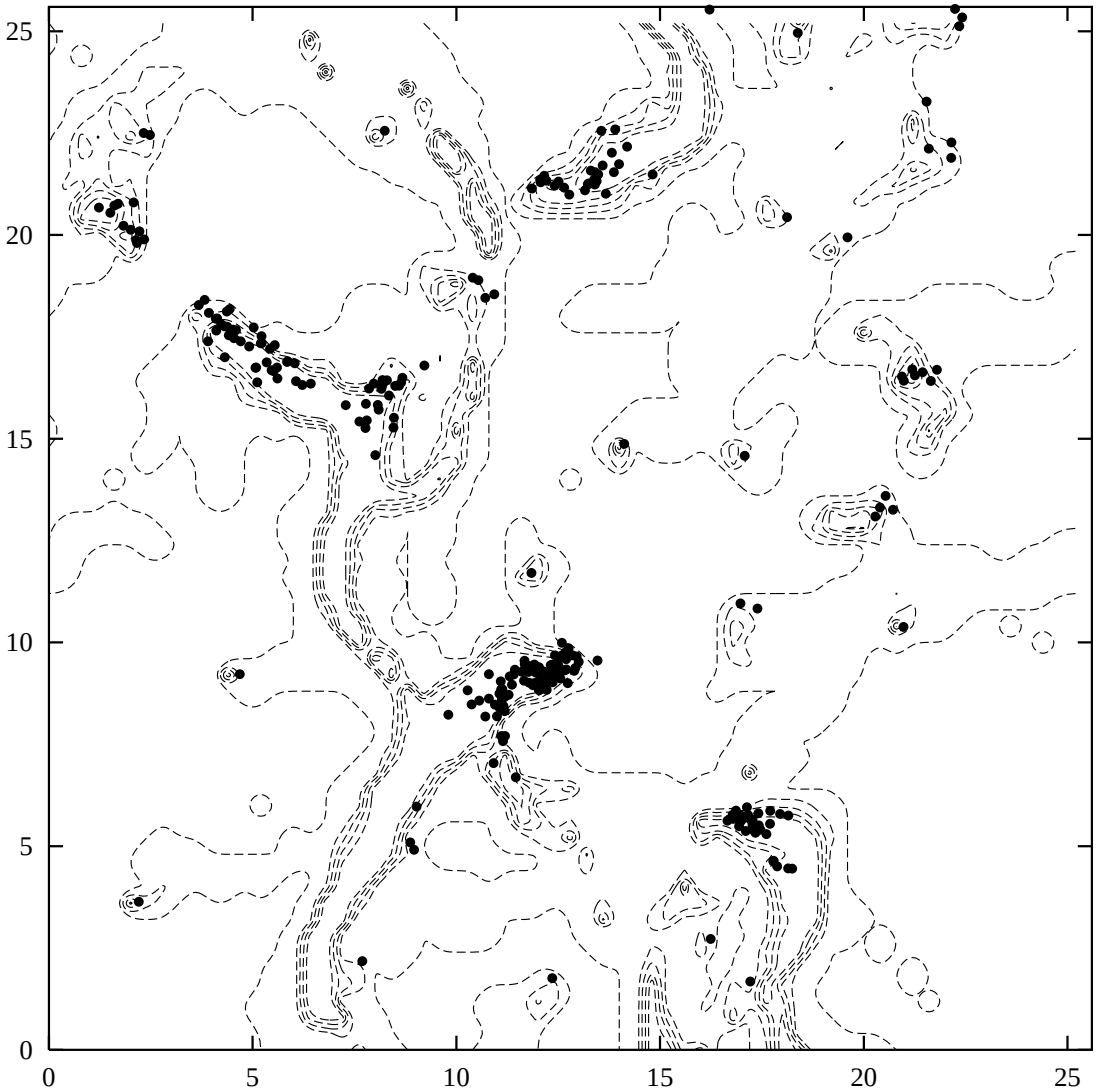

Figure 2.26: Phytoplankton concentration contoured from 0.2 by 0.2 to 0.8 with the zooplankton positions shown by dots. Parameters are $\mu = 0.2$, $g = 0.05$, $P_0 = 1$, $r = 1$, $\kappa = 0.014$, $V_0 = 0.2$.

Searching for food

As a final example, we consider how behavior which results in movement up the gradient of food concentration can alter the net grazing rate. In the previous discussion of taxis, we presumed that the organism could sense gradients in the cue field. However, animals can achieve much the same result by having a memory of past conditions and comparing them to present ones. Let us describe the state of each individual by its position, speed (relative to the water), direction, and a physiological variable, call it gut-fullness. The dynamics is described by

$$\begin{aligned} dX &= V\cos\theta\,\delta t \\ dY &= V\sin\theta\,\delta t \\ dV &= -\gamma(V - V_0)\,\delta t + s_v dR_1 \\ d\theta &= s_\theta\, dR_2 \\ dG &= -\lambda[G - P(X,Y,t)]\,\delta t \quad . \end{aligned}$$

The parameters V_0, s_v, and s_θ can depend on environmental (P) or internal (G) factors. The random increments dR_1, dR_2 have zero mean and variance $\sqrt{\delta t}$.

When the parameters are constant, the mean square displacement grows linearly with time

$$\frac{d}{dt}\langle (X - X_0)^2 + (Y - Y_0)^2\rangle = 4\left[\frac{V_0^2}{s_\theta^2} + \frac{s_v^2}{2\gamma(\lambda + \frac{s_\theta^2}{2})}\right]$$

For fixed P, the gut-fullness will limit to $G \to P$. If $G > P$, the organism had been in regions with greater food concentrations than it is now seeing. We shall show that if it turns more frequently under such conditions, it will migrate up the food gradient.

To demonstrate this, assume that s_θ is an increasing function $S(G - P)$ and that the physiological process is fast; then

$$G - P \simeq -\frac{1}{\lambda}\frac{D}{Dt}P \quad ,$$

and s_θ depends on gradients of P. The relevant Boltzmann equation,

$$\frac{\partial}{\partial t}\mathcal{P} + V\cos\theta\frac{\partial}{\partial x}\mathcal{P} + V\sin\theta\frac{\partial}{\partial y}\mathcal{P} = \gamma\frac{\partial}{\partial V}(V - V_0)\mathcal{P} + \frac{\partial^2}{\partial V^2}\frac{1}{2}s_v^2\mathcal{P} + \frac{\partial^2}{\partial\theta^2}\frac{1}{2}\left[S(-\frac{1}{\lambda}\frac{D}{Dt}P)\right]^2\mathcal{P} \quad ,$$

implies that the lowest order $\mathcal{P}$ has a Gaussian structure in V with mean V_0 and amplitude proportional to $[S(-\frac{1}{\lambda}\frac{D}{Dt}P)]^{-2}$. The expected biological velocity is

$$\mathbf{u}_{bio} = V_0\frac{\int d\theta(\cos\theta, \sin\theta)\left[S(-\frac{V_0}{\lambda}\cos\theta\frac{\partial}{\partial x}P - \frac{V_0}{\lambda}\sin\theta\frac{\partial}{\partial y}P)\right]^{-2}}{\int d\theta\left[S(-\frac{V_0}{\lambda}\cos\theta\frac{\partial}{\partial x}P - \frac{V_0}{\lambda}\sin\theta\frac{\partial}{\partial y}P)\right]^{-2}}$$

(assuming $\frac{\partial}{\partial t}P$ is small). At any particular point, the orientation of the axes is arbitrary so we can take $\frac{\partial}{\partial y}P = 0$; hence the integral with $\sin\theta$ will vanish, implying that the velocity is in the direction of the gradient of P. Furthermore, if $\frac{\partial}{\partial x}P > 0$, the denominator is largest for $\theta = \pi$ and smallest for $\theta = 0$, and the $\cos\theta$ integral will be positive – up-gradient movement (see figure 2.xx). Figure 2.xx shows example distributions of P and positions of the organisms in an experiment where the food is supplied in Gaussian blobs at random times. The food seen on average by the organisms is considerably higher than the average food over the domain (figure 2.xx). The mean grazing rate is on average twice the product of the mean P and Z values, with peaks well over three times that expected from the mean concentrations. Clearly the taxis behavior significantly increases the food-gathering ability.

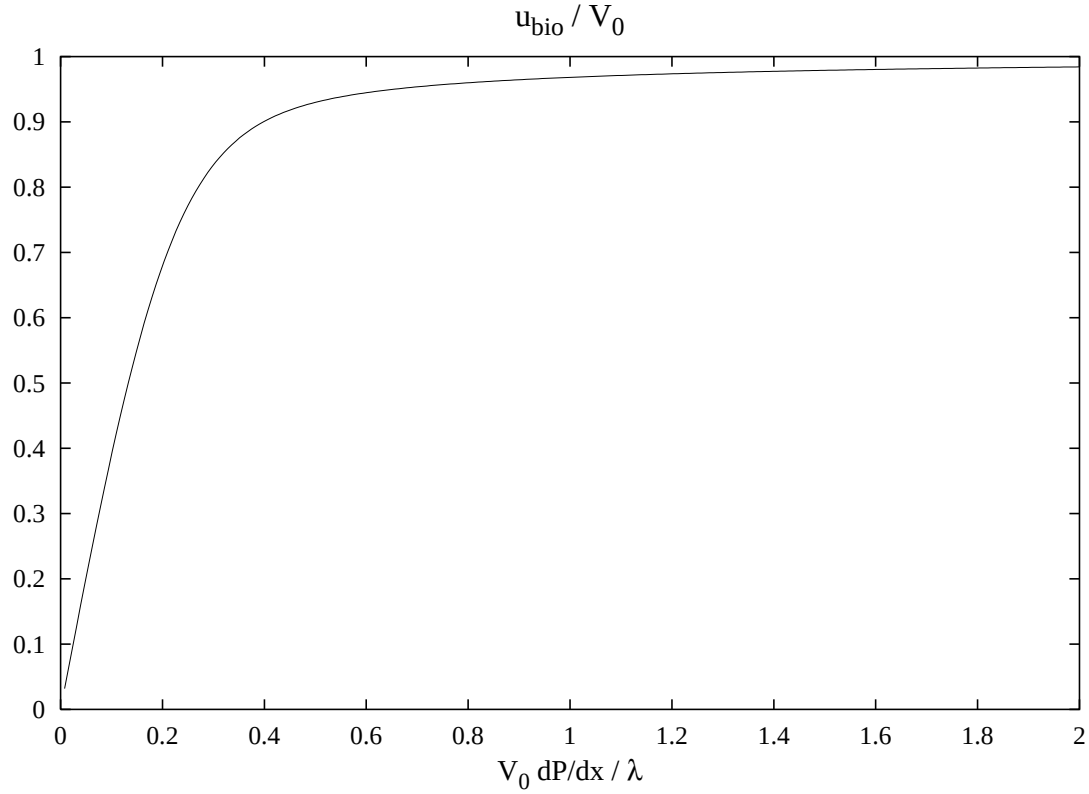

Figure 2.27: Estimated up-gradient velocity

These examples suggest that movement and patch formation can have significant effects on biological interactions. Frequently, these processes occur on scales smaller than those which the model of interest can resolve and therefore must be parameterized. Behavior adds another level of complexity to this ubiquitous problem: even when a single organism dominates Z and even when lab measurements of grazing rates exist, the average rate over a block of ocean can be significantly different because of patchiness and behavior.

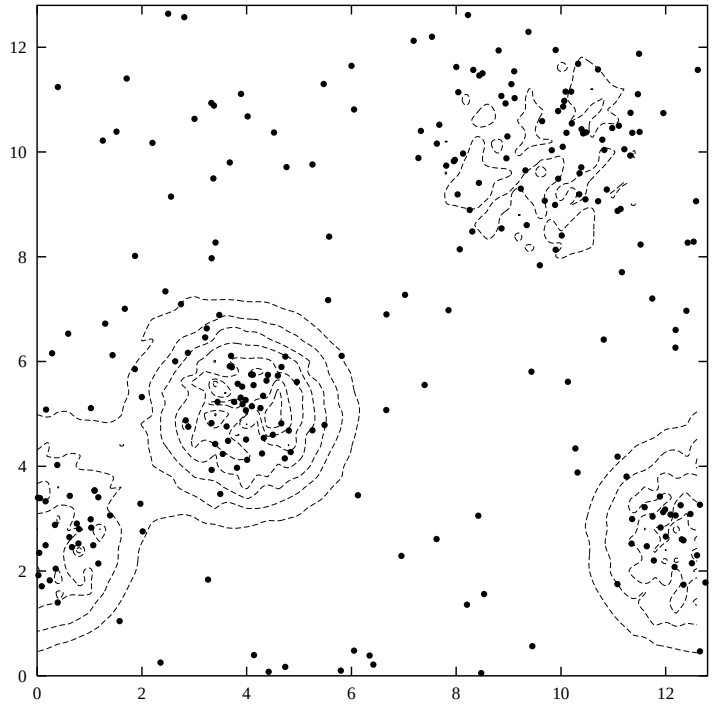

Figure 2.28: Contours of P (0.1 to 0.7) and positions of grazers at $t = 3000$. The upper right blob of P has been nearly consumed.

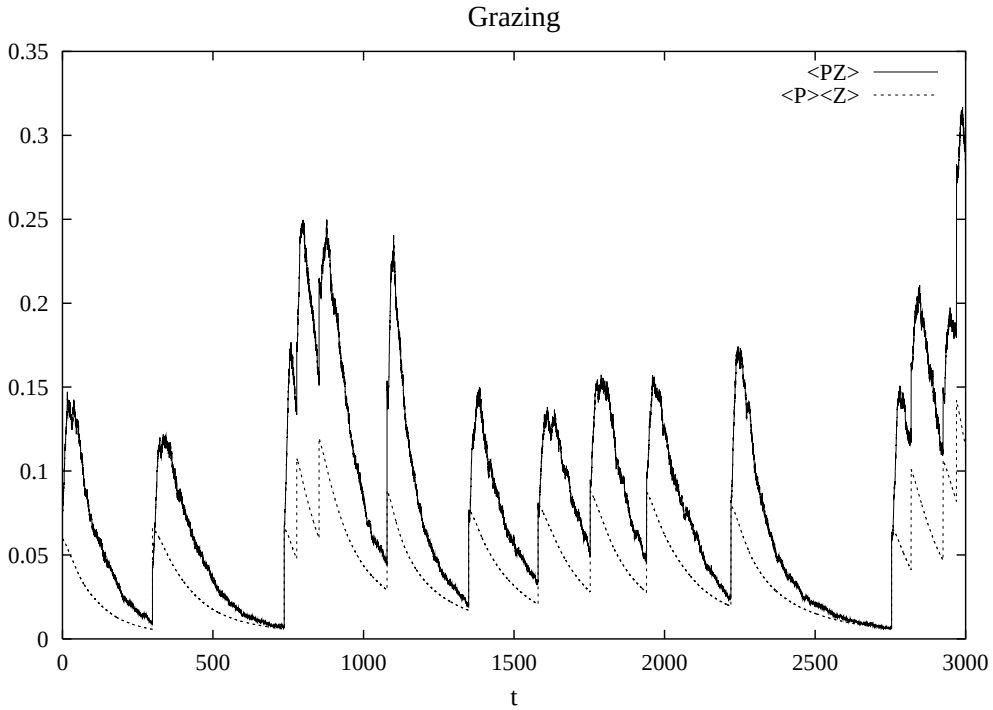

Figure 2.29: Average grazing rate $\langle PZ \rangle$ compared to the grazing rate estimated from the mean concentrations $\langle P \rangle \langle Z \rangle$

2.7 — Movement and flow

Our vertical migration example in section 2.xx demonstrates that the interplay between movement and diffusion leads to quite inhomogeneous distributions; we shall now consider how vertical swimming by the zooplankton alters the upwelling problem discussed in chapter xx. We assume that the flow is steady, but that the zooplankton have a constant vertical swimming velocity which is added to the motion produced by the fluid. Figures 2.xx-xx compare the distributions in three cases, $w_0 = 0$ and $\pm 1 \times 10^{-4}\ km/d$, while figure 2.xxa,b summarizes the peak and mean values. The peak Z values increase with either upward or downward swimming, but for entirely different reasons. In the upward swimming case, they concentrate near the surface just as in the one-dimensional case, but in the offshore waters. Likewise, N_t increases near the surface and decreases below. As a result, the net flux of N_t is out of the domain and its average value decreases (figure 2.xx). Concomitantly, the average value of Z also decreases (as it does in the zero-dimensional case when N_t goes down). Indeed, the average value of P increases, an effect not found in simpler situations. We can understand this from the linearized form of the Z equation

$$\frac{\partial}{\partial t}Z' + w\frac{\partial}{\partial z}\overline{Z} + \frac{\partial}{\partial z}w_0\overline{Z} = ag\overline{Z}P' \quad .$$

Both w and w_0 are positive, as is $\frac{\partial \overline{Z}}{\partial z}$; therefore, we expect that P' will be everywhere positive in equilibrium. Thus, the average P in the upwelling zone is higher (1.32) than in the case without flow (1.25) and increases further when the zooplankton swim upwards.

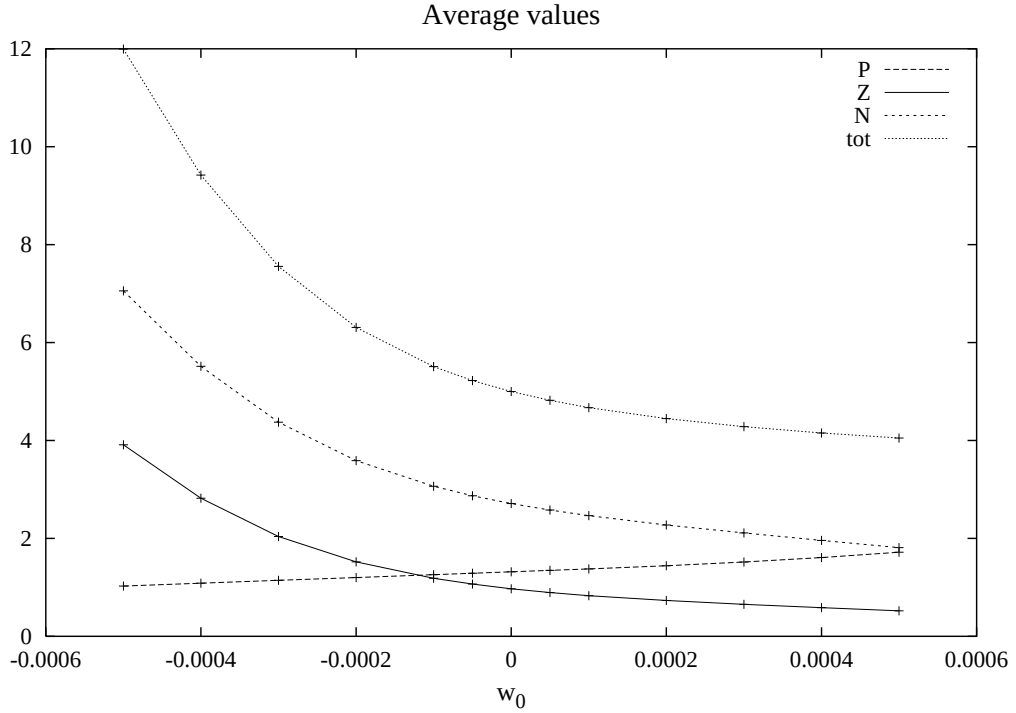

Figure 2.30: Average values of P, Z, N, and $N_t = P + Z + N$ over the upwelling domain as the zooplankton swimming velocity changes.

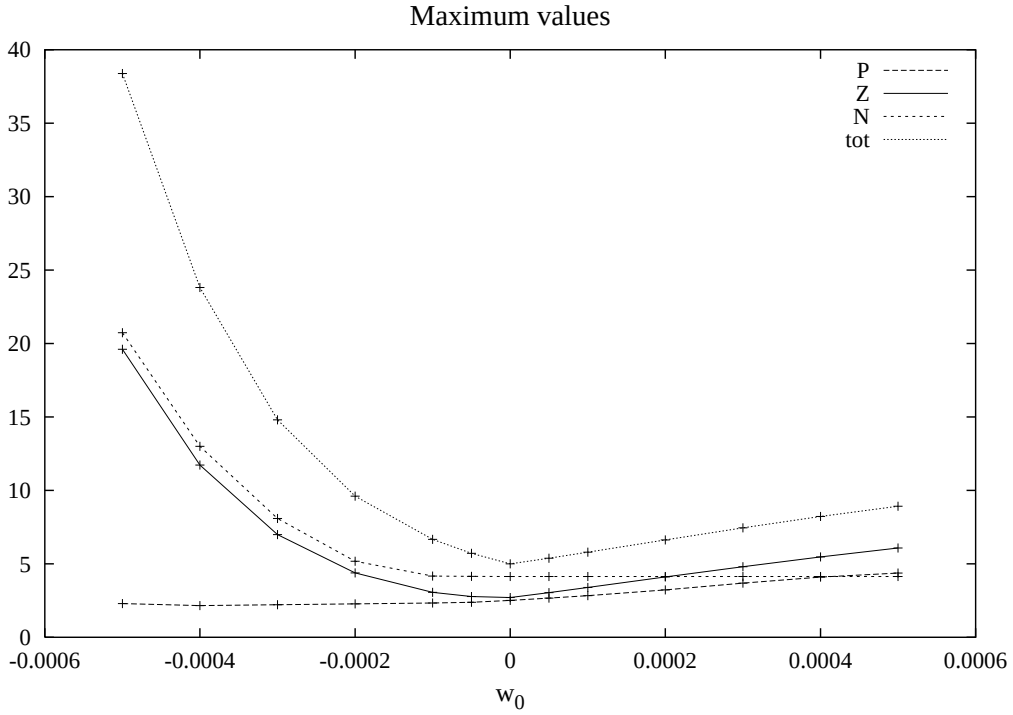

Figure 2.31: Maximum values. (For Z, the values in the corner have been excluded; they can be as much as 50% higher for the rapid downwelling case, but are not likely to be reliable numerically.)

The case of downwards swimming has the opposite effect on the average values of the fields: the outflowing surface water is depleted of N_t so that the total nitrogen increases within the domain, as does the average Z concentration. Correspondingly, the net amount of phytoplankton decreases. But the maximum values give quite a different picture (figure 2.xxb). Zooplankton swimming downwards get out of the offshore current and are transported back onshore and remain in the upwelling zone. Stommel (19xx) discussed some of the differences between the trajectories of sinking particles compared to those of fluid elements and showed that some particles could remain buoyed up by circulations such as Langmuir cells. Much the same argument applies here: some trajectories (figure 2.xx) form closed recirculation cells. The most obvious one is the point at which the horizontal velocity vanishes and the upwelling speed matches the downward swimming rate — the organism stays at the same geographic point. An animal slightly to the east descends, is carried to the west where the vertical velocity exceeds $|w_0|$, moves upwards and then to the east, where its downward swimming returns it to the initial position. To prove that the motion is indeed cyclic, note that the trajectories are determined by an effective streamfunction

$$\psi_Z = \psi - w_0 x \quad ,$$

with the stationary point (where by $\nabla\psi_Z = 0$) being a local minimum. In the vicinity of that point, ψ_Z will be a quadratic function, so that the lines of constant effective streamfunction form closed ellipses. For zooplankton further out, the ψ_Z contours will hit

the bottom; in the presence of mixing, the animals remain in the bottom layer and move up the slope into the surface ocean again.

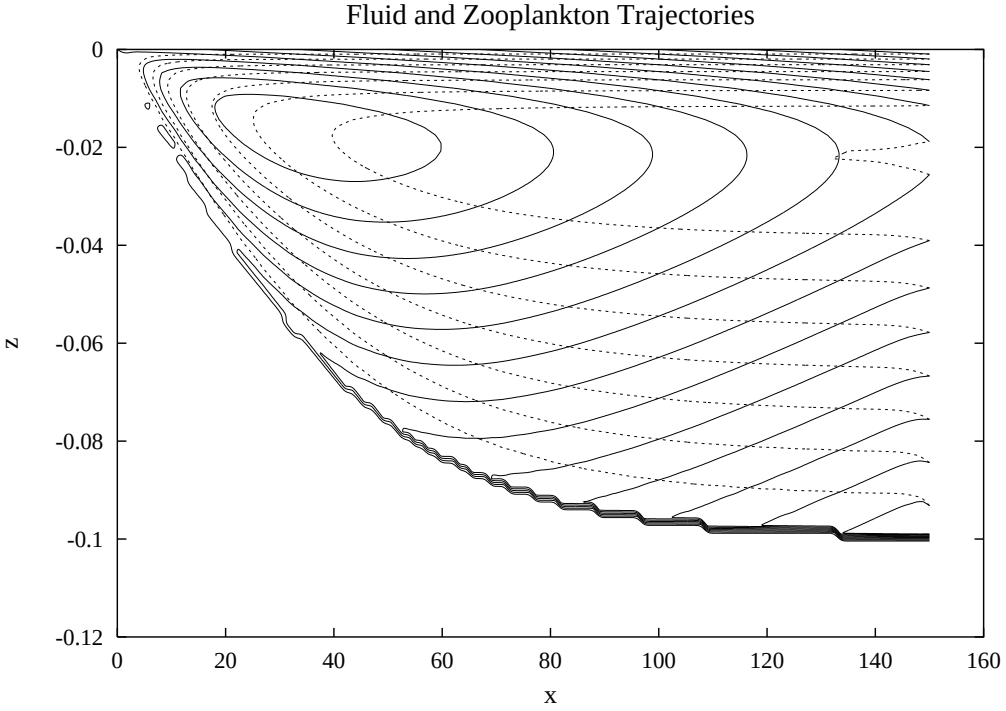

Figure 2.32: Zooplankton trajectories (solid) and fluid/ P/ N trajectories (dashed) for $w_0 = -3 \times 10^{-4}$ km/d.

The trajectory figure provides a handle on why the Z, N, and N_t values rise to large values: the flow provides a steady source of food for the zooplankton in the recirculating gyres, while removing the phytoplankton-depleted water. To see this, let us integrate the sum of the P and N equations over an area A enclosed by a contour of constant ψ_Z

$$\oint \mathbf{u} \cdot \hat{\mathbf{n}}(P+N) = -g \iint PZ + d_z \iint Z + \oint \kappa \hat{\mathbf{n}} \cdot \nabla(P+N) \quad .$$

(Strictly speaking, since the diffusion in this model is anisotropic, the last term is

$$\iint \frac{\partial}{\partial x_i} \kappa_{ij} \frac{\partial}{\partial x_j}(P+N) = \oint \hat{n}_i \kappa_{ij} \frac{\partial}{\partial x_j}(P+N)$$

but this does not change the argument.) Since $P+N$ is high in the deep water for the downward swimming case, the advective term is negative (and the diffusive term is relatively small) which implies the grazing term is larger than the zooplankton death term. But the zooplankton equation, integrated in the same way, implies

$$0 = g \iint PZ - d_z \iint Z + \oint \kappa \hat{\mathbf{n}} \nabla Z \quad .$$

Therefore the excess grazing must be balanced by diffusive losses out of the area; given weak diffusion, the gradients must become large and the peak values must be big. Indeed, calculations with a larger mixing rate do give weaker maxima.

We can also view the dynamics by considering what happens along a streamline in the case with $w_0 = 0$. As the parcel of fluid moves shoreward and up, the increasing light leads to N being incorporated into P and then, since $P > d_Z/ag$, to Z. This high Z, low N water washes out of the domain in the surface layer. But with $w_0 < 0$, the high Z concentrations are not transported out; instead they swim down into the incoming, high nutrient and high phytoplankton water which provide additional food for growth.

2.8 — Fluid Dynamics

We have discussed the transition from individuals to continuum models above; similar arguments can be made for the way in which collections of molecules behave like a classical fluid. Unlike the equations for taxis and kinesis (2.xx, xx), fluid dynamics requires prediction of the mean velocities as well as of the density. Continuum models of schooling organisms require similar information; so a brief discussion seems worthwhile.

Boltzmann (19xx) developed the basic approach for deriving the Navier-Stokes equations from molecular dynamics; the analysis was finally completed by Chapman (19xx) and Enskog (19xx) who derived the proper forms and values for viscosity and conductivity (c.f. Harris, 19xx). Here, we take a simplified approach akin to Bhatnager, Gross and Krook (19xx) or Welander (19xx) and assume that the stochastic interactions between molecules have two effects. First, they cause the individual velocities to relax back to the local mean, and, second, they generate thermal fluctuations which maintain variance in the velocities. Putting this *ansatz* into 2.xx resuilts in

$$\frac{\partial}{\partial t}\mathcal{P}_m = -\frac{\partial}{\partial x_i}(u_i\mathcal{P}_m) - \frac{\partial}{\partial u_i}(a_i\mathcal{P}_m + r[u_i - V_i]\mathcal{P}_m) + \frac{\partial^2}{\partial u_i^2}(rRT\mathcal{P}_m) \quad ,$$

where $\mathcal{P}_m(\mathbf{x}, \mathbf{v}, t) = Nm\mathcal{P}$ is the local mass density near $\mathbf{x}$ and $\mathbf{v}$ and $\mathbf{V}$ is the mean velocity

$$V_i = \int d\mathbf{u}\, u_i\mathcal{P}_m \Big/ \int d\mathbf{u}\mathcal{P}_m \quad or \quad \rho V_i = \int d\mathbf{u}\, u_i\mathcal{P}_m$$

with $\rho = \int d\mathbf{u}\, \mathcal{P}_m$. The a_i accelerations represent external forces such as gravity. The local solution to the Boltzmann-like equation – achieved to a good approximation when r is large – is a Maxwell distribution $\mathcal{P} = \rho\mathcal{G}(\mathbf{u} - \mathbf{V}|RT)$ with mean velocity $\mathbf{V}$ and mean temperature T. (Replacing the stochastic $\mathcal{K}$ by RT is really appropriate for gas dynamics, where it gives the correct velocity variance, rather than water and gives the proper velocity variance. Since we are simply trying to illustrate the way in which the Navier-Stokes equations arise, we will not be concerned about the differences between the two fluids.)

From the Boltzmann equation, we can find equations for the evolution of mass and momentum by integrating over $\mathbf{u}$ or multiplying by $\mathbf{u}$ and then integrating. The results are similar to previous ones, with the flux now written in terms of the mean velocity $\mathbf{J} = \rho\mathbf{V}$:

$$\frac{\partial}{\partial t}\rho + \nabla \cdot (\mathbf{V}\rho) = 0$$

$$\frac{\partial}{\partial t}V_i + V_j\nabla_j V_i + \frac{1}{\rho}\nabla_j\tau_{ij} = a_i$$

with the stresses given by $\tau_{ij} = \int d\mathbf{u}(u_i - V_i)(u_j - V_j)\mathcal{P}_m$. We arrive at the Euler equations by using $\mathcal{P} \simeq \rho\mathcal{G}(\mathbf{u} - \mathbf{V}|RT)$ to estimate $\tau_{ij} \simeq \rho\delta_{ij}RT = p\delta_{ij}$

$$\frac{\partial}{\partial t}\rho + \nabla\cdot(\mathbf{u}\rho) = 0$$
$$\frac{\partial}{\partial t}\mathbf{u} + (\mathbf{u}\cdot\nabla)\mathbf{u} = -\frac{1}{\rho}\nabla p + \mathbf{a} \quad .$$

If we incorporate corrections to the Maxwell distribution, we can expect to find a form of viscosity; to see this we multiply the Boltzmann equation by $u_j u_k$ and integrate

$$\frac{\partial}{\partial t}\rho V_j V_k + \frac{\partial}{\partial t}\tau_{jk} + \frac{\partial}{\partial x_i}\left(V_i V_j V_k\rho + V_i\tau_{jk} + V_j\tau_{ik} + V_k\tau_{ij} + \int u_i' u_j' u_k' \mathcal{P}_m\right)$$
$$= V_j a_k\rho + V_k a_j\rho - 2r\tau_{jk} + 2r\rho RT\delta_{jk} \quad .$$

We will substitute the lowest order approximation into the left-hand side, so that the third order term vanishes, and use the inviscid equations above to eliminate most of the terms

$$\frac{\partial}{\partial t}\tau_{jk} + \frac{\partial}{\partial x_i}[V_i\tau_{jk}] + \tau_{ik}\frac{\partial V_j}{\partial x_i} + \tau_{ij}\frac{\partial V_k}{\partial x_i} = -2r[\tau_{jk} - p\delta_{jk}] \quad .$$

If we now use the lowest order (for large r) result $\tau_{jk} = \rho RT\delta_{ij}$ and assume temperature is conserved, we are left with

$$\tau_{jk} = p\delta_{jk} - \eta\frac{1}{2}\left[\frac{\partial V_j}{\partial x_k} + \frac{\partial V_k}{\partial x_j}\right]$$

with $\eta = p/r$. If we use $r \sim rms(u')\sigma\rho/m$ where σ is the cross-section for collisions and m the mass of the molecule, η has the same form ($\propto \sqrt{T}$) as found by Chapman and Enskog. Note that the viscosity of water, unlike an ideal gas, decreases as temperature increases, we should not take the exact form of ν too seriously – as shown in fluid dynamics texts, the same form arises from macroscopic arguments together with the assumption that the stress / rate-of-strain relationship is linear and isotropic. Generally, we ignore gradients in η and work with the kinematic viscosity $\nu = \eta/\rho$, which, in turn, is treated as constant.

This derivation, then, shows that the Navier-Stokes momentum equations

$$\frac{\partial}{\partial t}V_i + V_j\nabla_j V_i = -\frac{1}{\rho}\nabla_i p + a_i + \nabla_j\nu\frac{1}{2}\left[\frac{\partial V_j}{\partial x_i} + \frac{\partial V_i}{\partial x_j}\right] \simeq -\frac{1}{\rho}\nabla_i p + a_i + \nu\nabla_j^2 V_i$$

appropriately represent the ways in which molecular collisions mix momentum within the flow. Henceforth, we shall use them in the Boussinesq form discussed in Chapter 1. x.xx)